# Axon guidance during mouse central nervous system regeneration is required for specific brain innervation

Céline Delpech, Julia Schaeffer, Noemie Vilallongue, Apolline Delaunay, Amin Benadjal, Beatrice Blot, Blandine Excoffier, Elise Plissonnier, Eduardo Gascon, Floriane Albert, et al.

Article

Developmental Cell

# Axon guidance during mouse central nervous system regeneration is required for specific brain innervation

## Graphical abstract

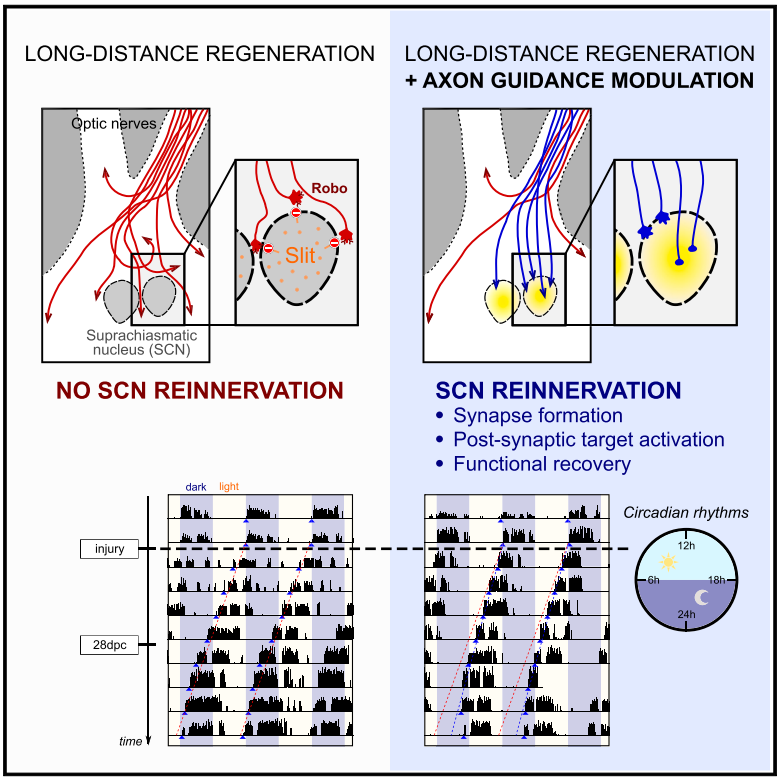


## Highlights

- In long-distance regeneration models, axons are misguided along the path
- Regenerating RGC avoid the suprachiasmatic nucleus due to Slit repulsive signaling
- *In vivo* silencing of Slit/Robo enables regenerating RGC to reinnervate the SCN
- The newly formed circuit sustains neuronal activation and behavioral recovery

## Authors

Céline Delpech, Julia Schaeffer, Noemie Vilallongue, ..., Stephane Belin, Alain Chédotal, Homaira Nawabi

## Correspondence

homaira.nawabi@inserm.fr

## In brief

Delpech et al. highlight that one barrier of neuronal circuit reconnection lies in incorrect pathfinding of regenerating axons in the mature brain. Using the retina/suprachiasmatic nucleus circuit, they show that manipulating guidance signals enables regenerating axons to reinnervate their initial brain target, with synapse formation, neuronal activation, and functional recovery.

Delpech et al., 2024, Developmental Cell *59*, 1–16
December 16, 2024 
https://doi.org/10.1016/j.devcel.2024.09.005

CellPress

Developmental Cell

CellPress
OPEN ACCESS

Article

# Axon guidance during mouse central nervous system regeneration is required for specific brain innervation

Céline Delpech,[1,6] Julia Schaeffer,[1,6] Noemie Vilallongue,[1,6] Apolline Delaunay,[1] Amin Benadjal,[2] Beatrice Blot,[1] Blandine Excoffier,[1] Elise Plissonnier,[1] Eduardo Gascon,[3] Floriane Albert,[1] Antoine Paccard,[1] Ana Saintpierre,[1] Celestin Gasnier,[1] Yvrick Zagar,[2] Valérie Castellani,[4] Stephane Belin,[1] Alain Chédotal,[2,4,5] and Homaira Nawabi[1,7,*]

[1]Université Grenoble Alpes, Inserm U1216, Grenoble Institut Neurosciences, 38000 Grenoble, France
[2]Sorbonne Université, INSERM, CNRS, Institut de la Vision, Paris, France
[3]Aix Marseille University, CNRS, INT, Institute of Neurosci Timone, Marseille, France
[4]University Claude Bernard Lyon 1, MeLiS, CNRS UMR5284, INSERM U1314, Lyon, France
[5]Institut de pathologie, groupe hospitalier Est, Hospices Civils de Lyon, Lyon, France
[6]These authors contributed equally
[7]Lead contact
*Correspondence: homaira.nawabi@inserm.fr
https://doi.org/10.1016/j.devcel.2024.09.005

## SUMMARY

Reconstructing functional neuronal circuits is one major challenge of central nervous system repair. Through activation of pro-growth signaling pathways, some neurons achieve long-distance axon regrowth. Yet, functional reconnection has hardly been obtained, as these regenerating axons fail to resume their initial trajectory and reinnervate their proper target. Axon guidance is considered to be active only during development. Here, using the mouse visual system, we show that axon guidance is still active in the adult brain in regenerative conditions. We highlight that regenerating retinal ganglion cell axons avoid one of their primary targets, the suprachiasmatic nucleus (SCN), due to Slit/Robo repulsive signaling. Together with promoting regeneration, silencing Slit/Robo *in vivo* enables regenerating axons to enter the SCN and form active synapses. The newly formed circuit is associated with neuronal activation and functional recovery. Our results provide evidence that axon guidance mechanisms are required to reconnect regenerating axons to specific brain nuclei.

## INTRODUCTION

In mammals, adult central nervous system (CNS) neurons are unable to regenerate after a lesion. This leads to permanent and irreversible loss of motor, sensory, and/or cognitive functions in patients affected by neurodegenerative diseases or traumatic injuries. The intrinsic regrowth properties of neurons themselves are largely responsible for this regeneration failure.[1] The visual system is one of the best models to study CNS axon regeneration. It is formed by the eyes, the optic nerve, and multiple brain nuclei that integrate and process visual information. In the retina, retinal ganglion cells (RGC) are the only output neurons that project their axon to the brain via the optic nerve. Upon optic nerve injury, RGC axon regrowth is triggered to some extent through the activation of developmentally or injury-regulated pathways, such as mTOR, JAK/STAT, and c-myc.[2–4] Moreover, the co-activation of such pathways leads to long-distance regeneration of some injured RGC, whose axons can regrow from the eye to the brain.[4–7]

However, regenerating axons are unable to reconnect their initial targets. Among the barriers to circuit functional reconnection, regenerating axons are misguided along their path and therefore cannot resume the initial circuit formed during development.[8] All models of regeneration developed so far, and particularly the long-distance ones, display major pathfinding errors in all regions of the nervous system,[9–12] contributing to functional recovery failure. Indeed, the minimum number of axons needed to connect the post-synaptic structures and ensure activation of the circuit has not been determined yet. Moreover, aberrant axonal projections can form deleterious circuits, potentially counteracting functional recovery attempts. For example, overexpression of the transcription factor Sox11 in corticospinal neurons improves corticospinal tract regeneration. However, the behavioral outcome worsens compared with the control, possibly because of inappropriate targeting of regenerating fibers.[13] Therefore, a major challenge stands out: how to drive regenerating axons to their correct target in order to restore function?

Axon guidance is a process well described during development, when millions of axons have to reach and make connections with target partners throughout the body. Their routes are strictly defined by specific expression of guidance cues at key

Please cite this article in press as: Delpech et al., Axon guidance during mouse central nervous system regeneration is required for specific brain innervation, Developmental Cell (2024), https://doi.org/10.1016/j.devcel.2024.09.005



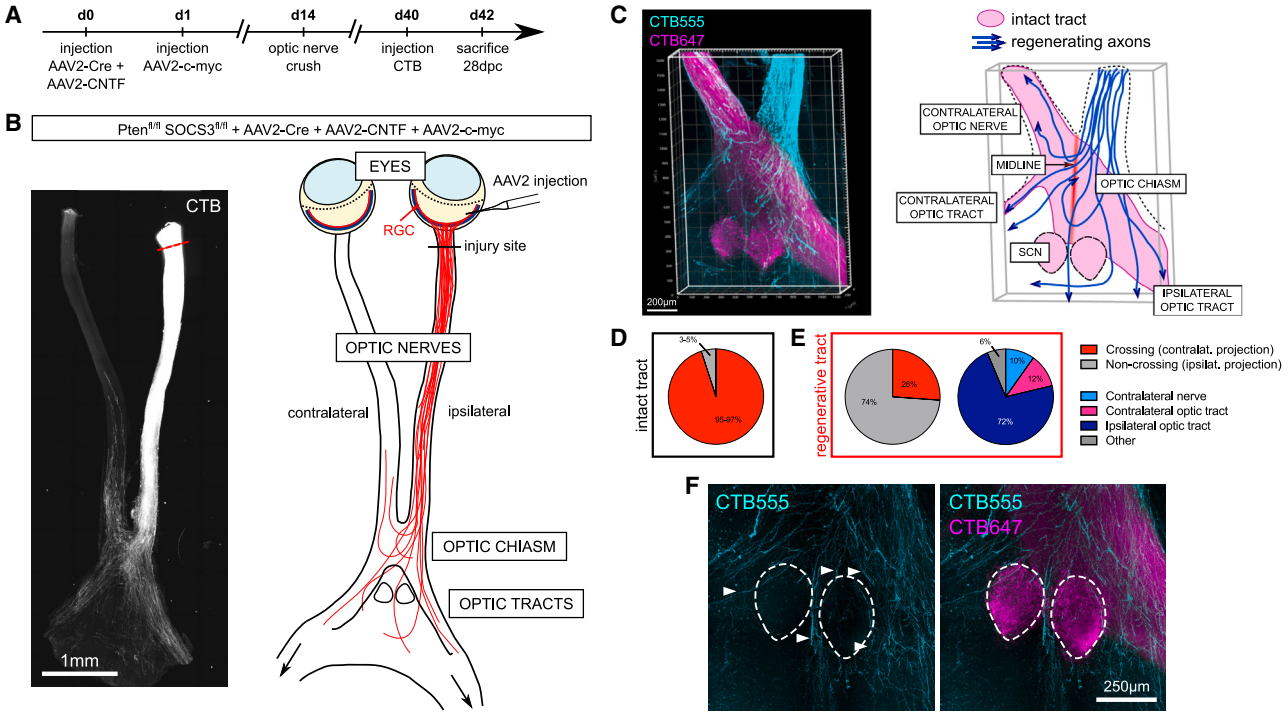


**Figure 1. Regenerating axons fail to reform the visual circuit**

(A) Timeline of long-distance regeneration experimental model in the mouse visual system.

(B) Confocal picture of whole optic nerves and optic chiasm 28 days post-unilateral ONC (28 dpc) in one $Pten^{fl/fl}SOCS3^{fl/fl}$ mouse eye injected with AAV2-Cre+AAV2-CNTF + AAV2-c-myc. Regenerating axons are traced using CTB (white). The red dashed line indicates the lesion site. Scheme of guidance defects observed in unilateral ONC: some axons turn back to the ipsilateral eye; others project to the contralateral optic nerve or get lost in the optic chiasm.

(C) 3D picture and scheme of whole optic nerves and optic chiasm 28 dpc in unilateral ONC. Regenerating axons are traced with CTB555 (cyan). Intact (contralateral) axons are traced with CTB647 (magenta).

(D) Proportion of midline crossing in intact circuit.

(E) Quantification of guidance defects observed in long-distance regeneration model: regenerating axons fail to resume the ipsi- versus contralateral distribution of the intact circuit.

(F) Confocal picture showing regenerating axons traced with CTB555 (cyan) and intact axons traced with CTB647 (magenta).

See also Figure S1.

choice points.[14] Guidance cues interact with receptors expressed on the growth cone of developing axons to shape their trajectories. Intermediate targets, such as the optic chiasm, for the visual system, are well-studied examples of critical decision-making points where such guidance mechanisms are at play. In the context of axon regeneration, regrowing axons face an environment very different from the embryonic one.[15] Yet, a growing body of evidence strongly suggests that guidance mechanisms also play a key role in adult CNS regeneration.[8,16] Our recent work shows that many guidance cues are expressed in the mature visual system, most of them known to be repulsive during development. Surprisingly, regenerating axons are able to respond to them, thereby opening the possibility to control their trajectories.[15]

In the present study, we use a long-distance regeneration model in the mouse visual system by co-activating mTOR, JAK/STAT, and c-myc pathways in RGC.[4] We observe that long-distance regrowing axons completely avoid the suprachiasmatic nucleus (SCN), one retinorecipient target of RGC that acts as the master regulator of circadian rhythms.[17] Based on a candidate approach, we show that the SCN expresses Slit guidance factors, known to act repulsively during development. Using a combination of *ex vivo* and *in vivo* approaches, we demonstrate that Slit signaling contributes to adult SCN reinnervation through the corresponding receptors, Robo1 and Robo2, expressed by regenerating RGC axons. Silencing Slit/Robo signaling leads to neuronal circuit formation in the long-distance regeneration model, with SCN activation at the cellular level but also with functional recovery. Altogether, our study demonstrates that axon guidance is required for functional circuit repair in the context of adult regeneration.

## RESULTS

### Regenerating axons display major guidance defects and avoid the SCN

To induce RGC axons' long-distance regeneration, we co-activated mTOR, JAK/STAT, and c-myc pathways via injection of adeno-associated virus serotype 2 (AAV2) expressing Cre,CNTF (ciliary neurotrophic factor) and c-myc in one eye of $Pten^{fl/fl}SOCS3^{fl/fl}$ mice, followed by optic nerve crush (ONC) injury (Figures 1A and 1B).[4] At 28 days post crush (28 dpc), RGC axons display robust regeneration along the optic nerve, up to the optic chiasm and beyond (Figure 1B). In intact wild-type (WT)

Please cite this article in press as: Delpech et al., Axon guidance during mouse central nervous system regeneration is required for specific brain innervation, Developmental Cell (2024), https://doi.org/10.1016/j.devcel.2024.09.005



CellPress
OPEN ACCESS

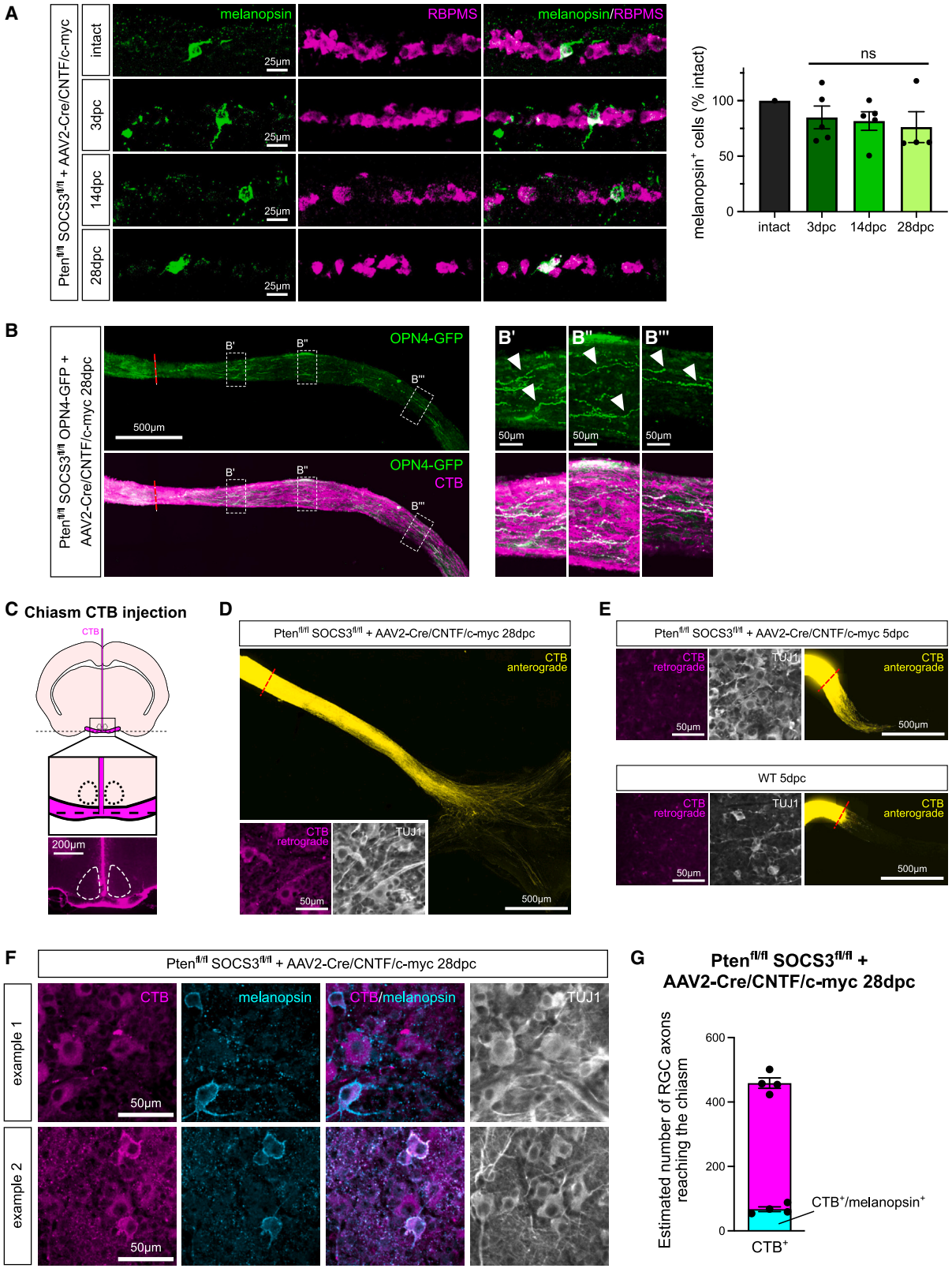


**Figure 2. ipRGC survive and regenerate in the long-distance regeneration model**

(A) Representative confocal pictures of retinal sections from Pten$^{fl/fl}$ SOCS3$^{fl/fl}$ eyes injected with AAV2-Cre + AAV2-CNTF + AAV2-c-myc (AAV2-Cre/CNTF/c-myc) in intact condition and at 3, 14, and 28 dpc. ipRGC are labeled with anti-melanopsin antibody (green) and RGC are labeled with anti-RBPMS (RNA-binding

*(legend continued on next page)*

condition (magenta, Figure 1C), 95% of RGC axons cross the midline to project contralaterally, while 5% project ipsilaterally (Figure 1D).[18] However, during regeneration, we observed multiple defects in the optic chiasm and in the SCN region (cyan, Figure 1C). For example, 74% of regenerating axons do not cross the midline, whereas 26% project contralaterally. Besides, 10% grow into the contralateral optic nerve (Figure 1E).

Strikingly, when we looked at the SCN region, we found that regenerating axons grow around and in-between the bilaterally symmetrical nuclei but do not enter them (Figure 1F). In the intact condition, in contrast to other retinorecipient brain nuclei, there is no specific topographic organization of retinal inputs in the SCN. It receives equal innervation from both eyes, mostly from M1-intrisically photosensitive RGC (ipRGC) and, to a lesser extent, by M2-ipRGC.[19,20] Normally, about 900 ipRGC innervate the SCN.[21,22] Interestingly, ipRGC axons can connect both SCN bilaterally by forming a colateral.[23] Thus, the intact eye was used to label both SCN via injection of fluorescently labeled cholera toxin B (CTB) (intact: magenta, regenerating: cyan; Figure 1F). We then asked whether the intact contralateral RGC axons could interfere with SCN innervation. We induced regeneration in one eye and injured both optic nerves (bilateral ONC) (Figure S1A). With this model, we observed similar axon pathfinding defects, although a higher proportion of regenerating axons cross the midline (49% in bilateral ONC versus 26% in unilateral ONC) and grow into the contralateral optic nerve and optic tract (35% versus 22%) (Figures S1B–S1F). This supports the notion that regenerating axons are guided by environmental cues, which, in this case, can be the growth-inhibitory myelin sheath of intact fibers[24,25] or differential mechanical stiffness imposed by space cluttering.[26] However, we found that regenerating axons still avoid entering the SCN, even with full denervation of both nuclei by RGC afferences upon bilateral ONC (Figures S1G and S1H). Thus, the presence of intact projections is not the cause of SCN reinnervation failure.

## ipRGCs are able to survive and to regenerate over long distances

The SCN is normally innervated by M1- and M2-ipRGC, which express high levels of the melanopsin photopigment.[27,28] We analyzed ipRGC survival based on melanopsin expression. In the long-distance regeneration model, 75% of melanopsin$^+$ RGC survive at 28 dpc (Figure 2A), consistent with previous studies describing ipRGC' strong resilience to axon injury.[29–31] Next, to assess ipRGC axon regeneration, we crossed Pten$^{fl/fl}$ SOCS3$^{fl/fl}$ mice with OPN4-GFP mice in which GFP is expressed specifically under the melanopsin (*Opn4*) promoter.[32] At 28 dpc, we observed GFP$^+$ fibers in the distal part of the optic nerve, showing that ipRGC axons are able to regenerate over long distances in the long-distance regeneration model (Figure 2B).

To quantify ipRGC regeneration into the chiasm, we set up a stereotaxic surgery to retrogradely label melanopsin$^+$-projecting RGC. In our long-distance regeneration model at 28 dpc, we injected CTB specifically in the optic chiasm (Figure 2C). We could observe CTB$^+$ RGC in the retina (regenerating side) at 28 dpc (Figure 2D). In contrast, no signal could be detected at 5 dpc (axons extending but not reaching the optic chiasm) nor in a WT injured retina (no regeneration) (Figure 2E), showing that only axons reaching the chiasm could take up the CTB. We found ~450 RGC, of which ~67 were melanopsin$^+$, growing their axon up to the chiasm (Figures 2F and 2G). These results confirm that ipRGC are able to survive and regenerate in the SCN vicinity, meaning that the SCN reinnervation failure is not due to impaired survival/regeneration of ipRGC, but rather that the SCN itself harbors an intrinsic repulsive activity.

## The SCN exerts a Slit-dependent repulsive activity on regenerating axons

To decipher this repulsive signaling, we conducted a screen of candidate canonical guidance cues in adult WT SCN (Figure S2A). In addition to cues found in our previous proteomics screen, such as NrCAM or PlexinA1,[15] we analyzed the expression of guidance molecules critical for visual system development, particularly in the developing optic chiasm,[33] using *in situ* hybridization. Interestingly, all members of the Slit family (*Slit1*, *Slit2*, and *Slit3*) are expressed in the intact adult SCN (Figure S2A). Their expression remains stable 28 days post-bilateral ONC (full RGC axons denervation of the SCN) (Figure S2A). We confirmed this result by RT-qPCR on RNA extracted from micro-dissected SCN in WT intact versus injured conditions. All three Slit family members show a stable mRNA expression in the SCN at 28 dpc (Figure S2B). We also confirmed that Slits are expressed in the SCN in the long-distance regeneration model (Figure 3A).

These guidance cues are good candidates to study the SCN repulsive potential. First, Slits act repulsively through their canonical receptors Robo1 and Robo2.[34] Second, during development, their suppression leads to similar guidance defects as in the regenerative model, with disorganized growth in the optic chiasm and projection to the contralateral optic nerve.[35] Thus, we hypothesized that Slits expressed in the SCN participate in its reinnervation failure via Robo receptors. We first analyzed *Robo1* and *Robo2* expression in mature intact and injured RGC. Using *in situ* hybridization, we showed that *Robo1* and *Robo2* are expressed in RGC and remain high at 28 dpc

protein with multiple splicing) antibody (magenta). Corresponding quantification of melanopsin$^+$ cell number, as a percentage of total ipRGC in intact condition. Data are expressed as mean ± SEM. Kruskal-Wallis test; ns, not significant.

(B) Confocal picture of optic nerve section from Pten$^{fl/fl}$SOCS3$^{fl/fl}$OPN4-GFP + AAV2-Cre/CNTF/c-myc at 28 dpc. ipRGC axons are GFP$^+$ (green). Regenerating axons are traced with CTB (magenta). The red dashed line indicates the lesion site. Arrowheads point to GFP$^+$ regenerating axons distal to the lesion site.

(C) Principle of CTB stereotaxic injection in the optic chiasm for regenerating axon backtracing.

(D) Confocal picture of whole optic nerve and optic chiasm showing regeneration tracing through CTB eye injection (yellow) and backtracing through CTB chiasm injection (magenta) to the retina.

(E) Control conditions with axons not reaching the chiasm at 5 dpc (Pten$^{fl/fl}$SOCS3$^{fl/fl}$ + AAV2-Cre/CNTF/c-myc and WT).

(F) Confocal pictures of whole-mount retinas labeled with anti-CTB antibody (magenta) and anti-melanopsin antibody (cyan), showing examples of melanopsin$^+$/CTB$^+$ RGC.

(G) Quantification of CTB$^+$ RGC estimated number per retina.

Please cite this article in press as: Delpech et al., Axon guidance during mouse central nervous system regeneration is required for specific brain innervation, Developmental Cell (2024), https://doi.org/10.1016/j.devcel.2024.09.005



CellPress
OPEN ACCESS

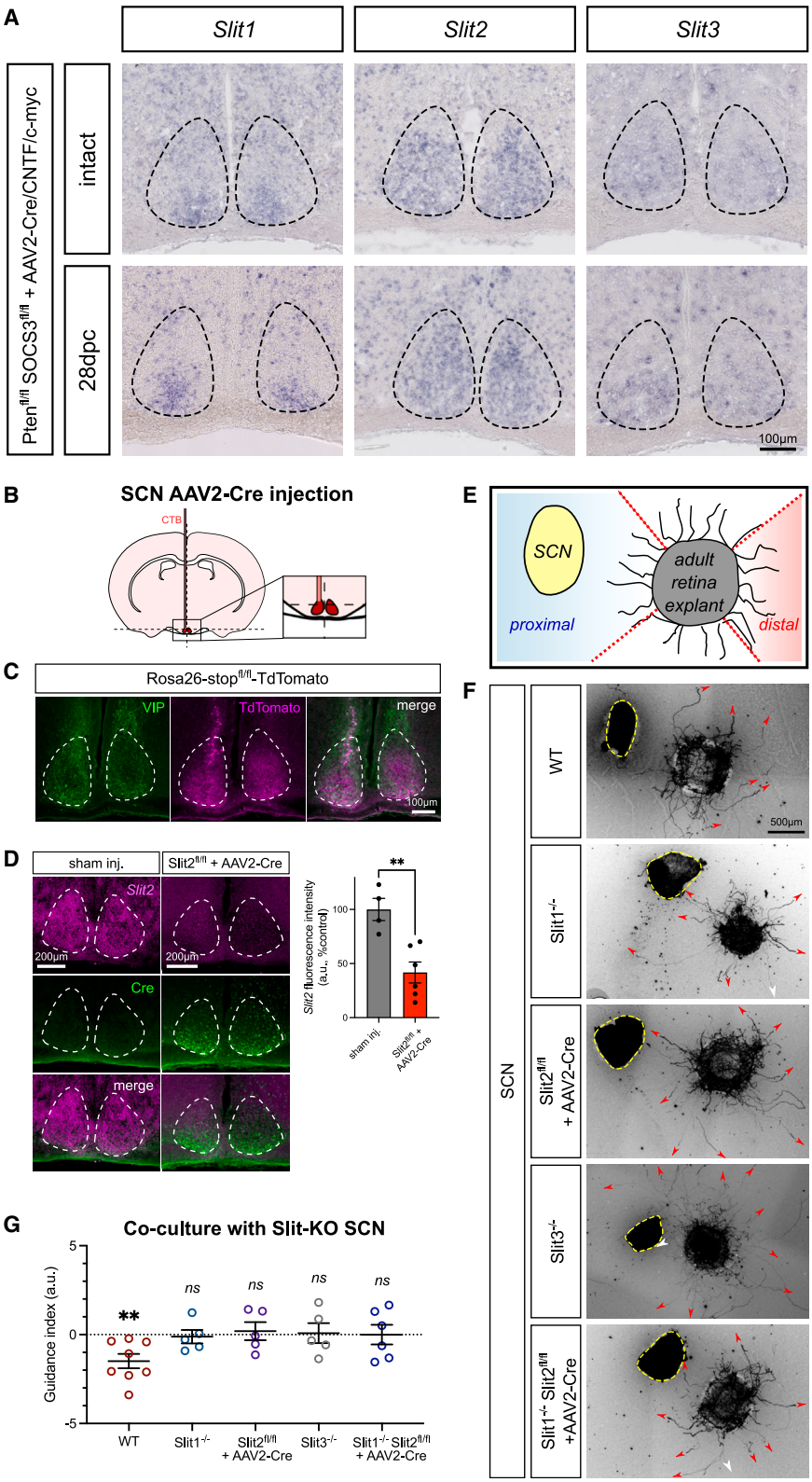


**Figure 3. The SCN exerts a Slit-dependent repulsive activity**

(A) *In situ* hybridization showing *Slit1*, *Slit2*, and *Slit3* expression in the SCN of Pten$^{fl/fl}$SOCS3$^{fl/fl}$ + AAV2-Cre/CNTF/c-myc. Expression is maintained at 28 dpc.

(B) Principle of SCN stereotaxic injection of AAV2-Cre.

(C) Control of SCN injection in Rosa26-stop$^{fl/fl}$-TdTomato mouse line, showing TdTomato expression (magenta) in the SCN labeled with anti-VIP antibody (green).

(D) *In situ* hybridization showing *Slit2* deletion in Cre-injected SCN of a Slit2$^{fl/fl}$ mouse (with Cre immunostaining) and corresponding quantification of *Slit2* fluorescence intensity. Data are expressed as mean ± SEM. Unpaired t test, $^{**}p$ value = 0.0039.

(E) Schematic of co-culture experiment.

(F) Representative pictures of a WT, Slit1$^{-/-}$, Slit2$^{fl/fl}$ + AAV2-Cre, Slit3$^{-/-}$ or Slit1$^{-/-}$Slit2$^{fl/fl}$ + AAV2-Cre SCN, co-cultured with a retinal explant from Pten$^{fl/fl}$ SOCS3$^{fl/fl}$ + AAV2-Cre/CNTF/c-myc.

(G) Corresponding quantification of guidance index showing the log-ratio of axon growth in the proximal versus the distal area. A negative guidance index indicates a significantly repulsive activity, while a null guidance index indicates a neutral activity.

Data are expressed as mean ± SEM. One-sample t test compared with zero, $^{**}p$ value = 0.0079; ns, not significant. See also Figures S2 and S3.

Please cite this article in press as: Delpech et al., Axon guidance during mouse central nervous system regeneration is required for specific brain innervation, Developmental Cell (2024), https://doi.org/10.1016/j.devcel.2024.09.005



(Figures S2C and S2D). In particular, melanopsin$^+$ RGC express *Robo1* and *Robo2* (Figures S2E and S2F). Additionally, we used organotypic cultures of adult retinal explants from the long-distance regeneration model[36] (Figure S2G) to decipher Robo1 and Robo2 expression within growth cones. Using high-resolution imaging on fixed cultures, we showed that Robo1 and Robo2 are both expressed on growth cones of regenerating axons (Figure S2H), suggesting that regenerating axons, including ipRGC, have the molecular tools to respond to Slits.

Next, we set up co-cultures of retinal and adult SCN explants in order to decipher SCN impact on the regenerating axons' behavior. As observed *in vivo* (Figures 1F and S1G), WT (Slit-expressing) SCN exerts a repulsive activity on regenerating axons from retinal explants (Figures 3E–3G). To investigate whether this repulsive activity is mediated by Slits, we manipulated Slit expression in the SCN and analyzed RGC axons guidance response. For this purpose, we used Slit1- and Slit3-full knockout mice. As Slit2-knockout is embryonic lethal,[37] we induced Slit2-specific knockdown via targeted injection of AAV2-Cre in the SCN of Slit2$^{fl/fl}$ mice. As a control, we performed AAV-Cre injection in the SCN of TdTomato reporter mice (Figure 3C). We show that Cre expression is effective in the SCN (labeled with SCN-specific marker vasoactive intestinal peptide [VIP]). Slit2-knockdown was verified by fluorescent *in situ* hybridization on SCN sections (~60% decrease) (Figure 3D). Knockout of any Slit alone, or combined knockout of Slit1 and Slit2, resulted in the loss of SCN repulsive activity, as axons grow in any direction, including toward Slit-deprived SCN (Figures 3F and 3G). Of note, we could not get any Slit1$^{-/-}$ Slit2$^{fl/fl}$ Slit3$^{-/-}$ samples, as mice could not survive the stereotaxic injection, suggesting that Slit1/Slit3 co-deletion is somehow detrimental.

Deletion of any Slit abolishes the SCN repulsive effect, suggesting that all three Slits are necessary to account for it. To confirm this, we set up an additional co-culture experiment, using COS cells expressing one or several Slits and the same retinal explants as previously (Figures S3A–S3C). We found that each Slit on its own has no significant repulsive effect, but only the combination of the three repels regenerating axons (Figures S3D–S3F). This effect is consistent with the synergistic or collaborative effect observed for Slit family members during development,[35,38,39] an effect that may be exacerbated in the case of adult regenerating axons. We concluded that Slit family members contribute to SCN repulsive activity and may account for its reinnervation failure *in vivo*.

## Slit/Robo signaling modulation *in vivo* makes regenerating axons enter the SCN

To modulate Slit guidance signaling *in vivo*, we deleted Robo1 and Robo2 expression in RGC. In a WT background, we found that Robo1/2 deletion does not induce any significant axon regeneration at 14 dpc (Figures S4A–S4C). Hence, Robo themselves do not have an intrinsic regenerative effect on RGC axons.

Next, we crossed Pten$^{fl/fl}$ SOCS3$^{fl/fl}$ mice with Robo1$^{-/-}$ and/or Robo2$^{fl/fl}$ mice to modulate each or both receptor(s) in combination with long-distance regeneration of RGC. As previously, we injected AAV2-Cre/CNTF/c-myc in one eye and performed bilateral ONC. Focusing on SCN reinnervation, we quantified the number of axons entering both SCN. In the case of single Robo modulation, we observed no significant effect of Robo1 deletion only (53 ± 4 intersects in Pten$^{fl/fl}$ SOCS3$^{fl/fl}$ Robo1$^{-/-}$ versus 37 ± 5 intersects in Pten$^{fl/fl}$ SOCS3$^{fl/fl}$) (Figures S4D, S4F, and S4G), and a modest increase in the number of SCN-entering axons in the case of Robo2 deletion only (77 ± 8 intersects in Pten$^{fl/fl}$ SOCS3$^{fl/fl}$ Robo2$^{fl/fl}$) (Figures S4E–S4G). Strikingly, when both Robo1 and Robo2 are knocked out, we observed a strong and significant increase in the number of regenerating axons entering both SCN (134 ± 12 intersects in Pten$^{fl/fl}$ SOCS3$^{fl/fl}$ Robo1$^{-/-}$ Robo2$^{fl/fl}$) and, notably, the ipsilateral one (104 ± 10 intersects) (Figures 4A–4C). We used three-dimensional (3D) imaging and reconstruction to specifically trace regenerating axons that enter and stay in the SCN without crossing it. In control conditions, axons clearly avoid the SCN. Strikingly, Robo1/Robo2 co-deletion leads to SCN reinnervation (Figures 4D and 4E; Videos S1 and S2). Although this analysis is limited by the inability to determine from fixed tissues whether these axons actually stay or keep growing, it brings striking evidence that SCN reinnervation *in vivo* is controlled by guidance mechanisms involving cues such as Slit/Robo.

In order to determine whether regenerating ipRGC could enter the SCN, we crossed Pten$^{fl/fl}$ SOCS3$^{fl/fl}$ OPN4-GFP mice with Robo1$^{-/-}$ Robo2$^{fl/fl}$ mice. Using immunofluorescence on SCN longitudinal sections, we detected CTB$^+$/GFP$^+$ fibers in the SCN (Figures 4F and 4G), showing that regenerating ipRGC are able to enter the SCN upon Robo1/2 modulation. Altogether, these results demonstrate that (1) adult regenerating RGC can be guided in regenerative conditions and (2) modulation of specific guidance signaling allows regenerating axons to enter the SCN.

## Axons entering the SCN are able to make synapses

To evaluate neuronal circuit reformation, we asked whether SCN-entering regenerating axons could form synapses in the SCN. For this purpose, we stained SCN sections for pre-synaptic marker VGLUT2, expressed in ipRGC-SCN glutamatergic synapses,[23,40] and post-synaptic marker PSD95 (postsynaptic protein 95). Using high-resolution imaging, we found VGLUT2$^+$ synapses in CTB$^+$ fibers that were directly adjacent to a PSD95$^+$ post-synaptic compartment, suggestive of synapses formed by regenerating fibers in the SCN (Figure 5A), despite limitations in spatial resolution of such imaging.

To confirm whether regenerating axons can make functional synapses with SCN neurons, we took advantage of monosynaptic pseudotyped EnvA rabies viruses expressing the GFP protein (EnvA-ΔG-RV-GFP), a viral vector known to be transported retrogradely via functional synapses and widely used to trace neuronal circuits *in vivo*. In these experiments, we first injected an AAV2-Cre expressed under VIP promoter (pVIP-Cre) and an adjuvant AAV required to deliver the TVA receptor (enabling the entrance of the EnvA-ΔG-RV-GFP vector into the target cells. TVA is the cellular receptor for subgroup A avian leukosis viruses) as well as the rabies glycoprotein (necessary for the transsynaptic transport)[41] (AAV2-TVA-RG) (Figures 5B and 5C). The SCN-specific Cre expression was confirmed using injection in Rosa26-stop$^{fl/fl}$-TdTomato mice (Figures 5D and 5E). We next validated that our monosynaptic vector had no leak. For this, we injected the EnvA-ΔG-RV-GFP in the absence of adjuvant AAV. As expected, we did not detect any GFP signal, indicating that pseudotyped rabies vectors were not able to infect the SCN

Please cite this article in press as: Delpech et al., Axon guidance during mouse central nervous system regeneration is required for specific brain innervation, Developmental Cell (2024), https://doi.org/10.1016/j.devcel.2024.09.005



CellPress
OPEN ACCESS

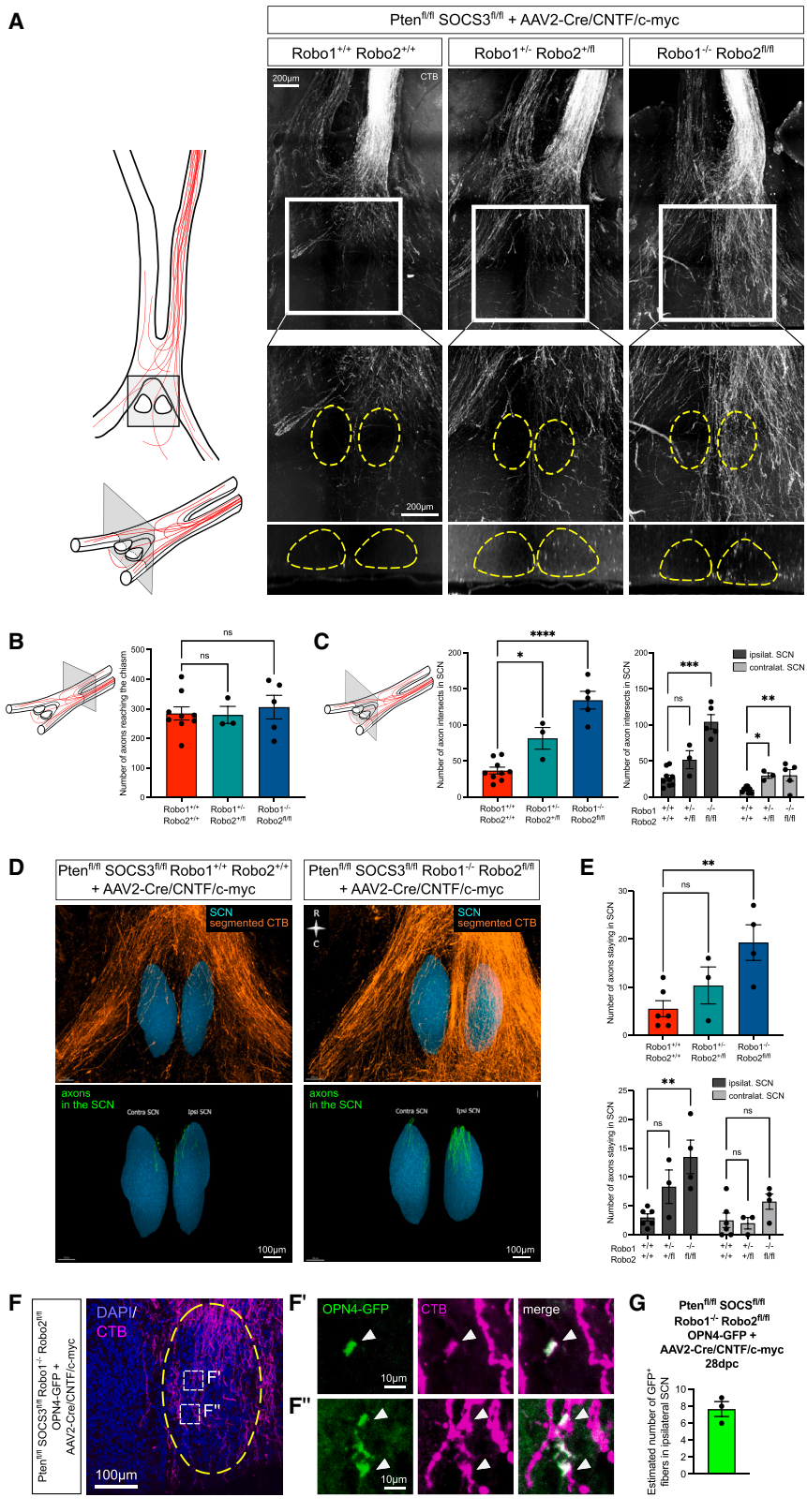


**Figure 4. Silencing Slit/Robo signaling *in vivo* promotes entry of regenerating axons into the SCN**

(A) Confocal picture of whole optic nerves and optic chiasm at 28 dpc in Pten$^{fl/fl}$SOCS3$^{fl/fl}$Robo1$^{+/+}$ Robo2$^{+/+}$, Pten$^{fl/fl}$SOCS3$^{fl/fl}$Robo1$^{+/-}$ Robo2$^{+/fl}$ and Pten$^{fl/fl}$SOCS3$^{fl/fl}$Robo1$^{-/-}$Robo2$^{fl/fl}$ mice, with unilateral injection of AAV2-Cre/CNTF/c-myc and bilateral ONC. Regenerating axons are traced using CTB (white). Pictures are representative of $N = 3–9$ animals in each condition. Zoom pictures: the SCN is indicated with the yellow dashed line (maximum projection and XZ orthogonal section panels).

(B) Quantification of the number of axons reaching the chiasm. Data are expressed as mean ± SEM. One-way ANOVA with Dunnett's correction; ns, not significant.

(C) Left: quantification of the number of axons entering the SCN. Data are expressed as mean ± SEM. One-way ANOVA with Dunnett's correction, ***$p$ value = 0.0004; ns, not significant. Right: distribution of axons entering the ipsilateral and contralateral SCN. Data are expressed as mean ± SEM. One-way ANOVA with Dunnett's correction, **$p$ value = 0.0065, ***$p$ value = 0.0003; ns, not significant.

(D) 3D imaging and reconstruction of regenerating axons in the SCN region at 28 dpc in Pten$^{fl/fl}$SOCS3$^{fl/fl}$ Robo1$^{+/+}$Robo2$^{+/+}$ + AAV2-Cre/CNTF/c-myc or Pten$^{fl/fl}$SOCS3$^{fl/fl}$Robo1$^{-/-}$Robo2$^{fl/fl}$ + AAV2-Cre/CNTF/c-myc.

(E) Top: quantification of the number of axons staying in the SCN. Data are expressed as mean ± SEM. One-way ANOVA with Dunnett's correction, **$p$ value = 0.0082; ns, not significant. Bottom: distribution of axons staying in the ipsilateral and contralateral SCN. Data are expressed as mean ± SEM. One-way ANOVA with Dunnett's correction, **$p$ value = 0.0047; ns, not significant.

(F) Confocal pictures of the ipsilateral SCN in Pten$^{fl/fl}$SOCS3$^{fl/fl}$Robo1$^{-/-}$Robo2$^{fl/fl}$OPN4-GFP + AAV2-Cre/CNTF/c-myc at 28 dpc. Arrowheads point to GFP$^+$/CTB$^+$ fibers in the SCN, indicating that OPN4-GFP$^+$ ipRGCs enter the SCN in Robo-knockout condition at 28 dpc.

(G) Corresponding quantification of GFP$^+$ fibers estimated number in ipsilateral SCN.

See also Figure S4 and Videos S1 and S2.

Please cite this article in press as: Delpech et al., Axon guidance during mouse central nervous system regeneration is required for specific brain innervation, Developmental Cell (2024), https://doi.org/10.1016/j.devcel.2024.09.005



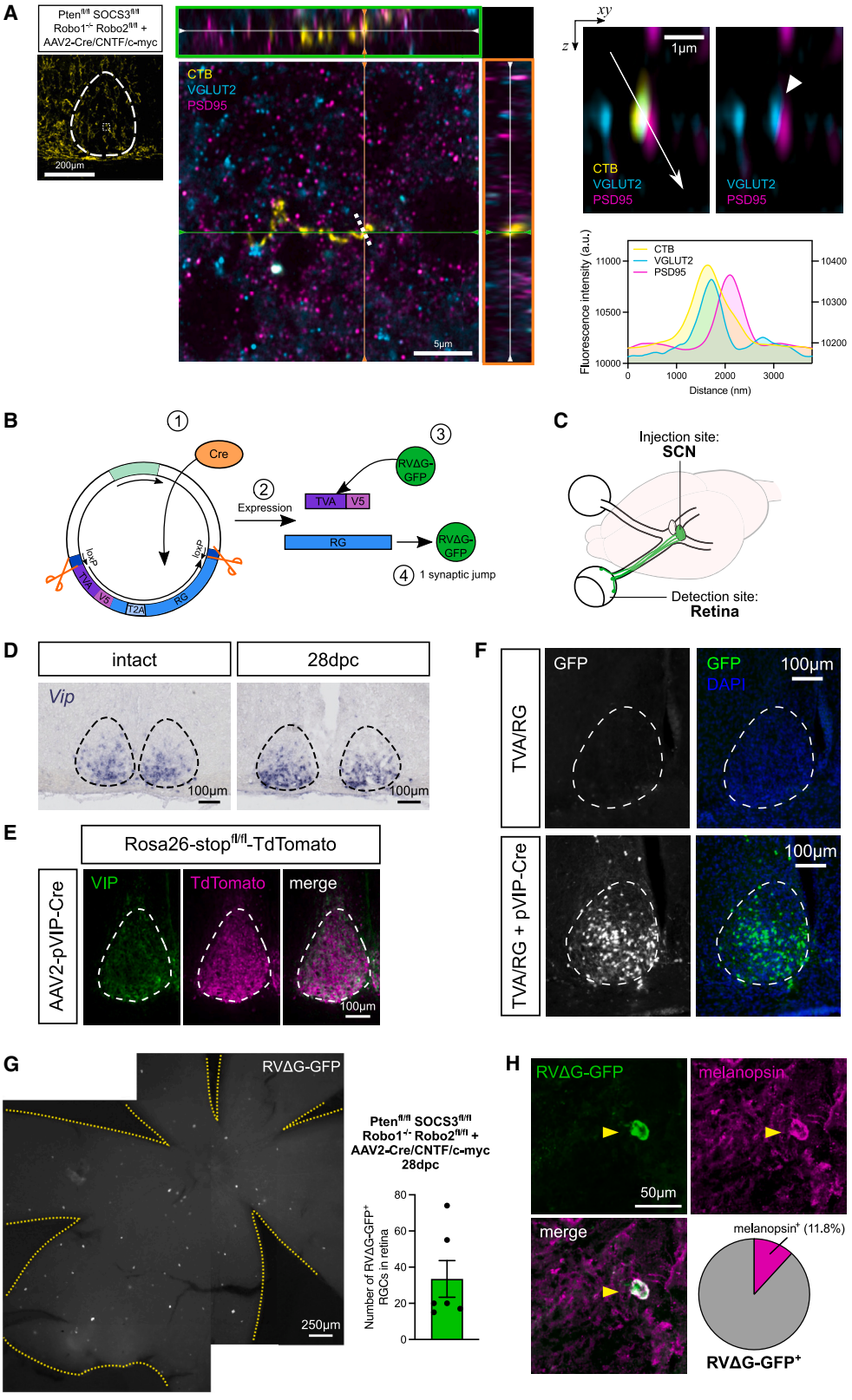


**Figure 5. Regenerating axons reinnervating the SCN form synapses**

(A) Left: confocal picture of the ipsilateral SCN from a Pten$^{fl/fl}$SOCS3$^{fl/fl}$Robo1$^{-/-}$Robo2$^{fl/fl}$ + AAV2-Cre/CNTF/c-myc at 28 dpc. Center: 3D confocal picture with Airyscan of an individual regenerative fiber forming a synapse in the SCN. The pre-synaptic compartment marker VGLUT2 (cyan) colocalizes with the CTB$^{+}$ fiber

*(legend continued on next page)*

in the absence of the TVA receptor. We then examined whether our monosynaptic tracing strategy was efficient. We initially confirmed that starter cells (GFP$^+$ cells) were restricted to the SCN. EnvA-ΔG-RV-GFP was injected in WT SCN 2 weeks after AAV2-TVA-RG + AAV2-pVIP-Cre injection. Cre expression, driven by the pVIP, enabled GFP expression. More importantly, GFP$^+$ cells were restricted to the SCN, indicating that RV can be internalized only by TVA-expressing cells in this area and validating our experimental approach (Figure 5F). Then, in Pten$^{fl/fl}$ SOCS3$^{fl/fl}$/Robo1$^{-/-}$ Robo2$^{fl/fl}$ mice 2 weeks post injury, we injected AAV2-TVA-RG + AAV2-pVIP-Cre. After 1 week, we injected the EnvA-ΔG-RV-GFP. If regenerating RGC axons have formed functional synapses into the SCN, the monosynaptic RV should be retrogradely transported into the RGC cell bodies. 1 week after RV-injections, we dissected the retinas and found RGC expressing the GFP (about 30 per retina, Figure 5G). This result confirmed that regenerating axons with Robo1/2 modulation are able not only to enter but also to establish functional connections onto SCN neurons.

To determine whether ipRGC are connected to the SCN, we stained GFP$^+$ RGC for melanopsin (Figure 5G). We found GFP$^+$/melanopsin$^+$ RGC in the retina, showing that ipRGC are connecting the SCN (as hinted by Figures 4G and 4H). Interestingly, we found that other RGC subpopulations are also primed to reinnervate the SCN upon Robo modulation. We focused on RGC subpopulations that have the highest survival rate in Pten$^{fl/fl}$ SOCS3$^{fl/fl}$ Robo1$^{-/-}$ Robo2$^{fl/fl}$ mice at 28 dpc, which include alpha-RGC (NF-H$^+$, osteopontin$^+$) and on-off direction-sensitive RGC (ooDSGCs, CART$^+$) (Figures S5A and S5B), consistent with previous work.[42] Besides ipRGC, we found that alpha-RGC, and ooDSGC to a lesser extent, can reinnervate the SCN upon Robo1/2 modulation (Figure S5C). Altogether, our results demonstrate that Slit/Robo signaling controls SCN innervation during regeneration.

## SCN reinnervation upon Robo modulation is associated with restoration of neuronal circuit activation

As synapses were found in the SCN, we then asked whether the newly formed neuronal circuit was functional in response to direct light activation. For this purpose, we set up a neuronal activity assay, based on expression of the immediate early gene c-fos in response to short light exposure (Figure 6A). c-fos expression is triggered specifically in the SCN of WT intact mice exposed to light for 30 min in the night (dark) phase, both in terms of number of activated neurons and of c-fos intensity (Figure S6A). In contrast, c-fos expression is not detected in non-photo-induced animals. Moreover, c-fos expression is not induced upon bilateral ONC, where RGC-to-SCN connections are lost (Figure S6A). In the long-distance regeneration model, we compared c-fos activation upon Robo1/2 modulation (Robo1$^{+/-}$ Robo2$^{+/fl}$ and Robo1$^{-/-}$ Robo2$^{fl/fl}$) versus control (Robo1$^{+/+}$ Robo2$^{+/+}$). Upon photo-induction at 28 dpc, we found a significant increase in the number of c-fos$^+$ cells in the SCN and a significant increase of c-fos intensity (Figures 6B and 6C). Because Robo2 knockout also induced a modest SCN innervation (Figures S4F and S4G), we assessed c-fos expression in Robo2$^{-/-}$ condition and found a significant increase in c-fos intensity compared with Robo2$^{+/+}$ (Figure S6B). Altogether, these results strongly suggest that SCN reinnervation by regenerating axons leads to specific activation in target cells upon light exposure, both in terms of c-fos$^+$ cell number and c-fos intensity (Figure 6C).

To further challenge this result, we performed two additional experiments. First, we asked whether activated SCN neurons were functionally connected by regenerating axons. To this end, we stained the SCN innervated by Robo1$^{-/-}$ Robo2$^{-/-}$ regenerating axons for synaptic markers and c-fos. Using high-resolution microscopy, we detected the presence of synapses (VGLUT2$^+$/PSD95$^+$ adjacent compartments) from CTB$^+$ fibers and activated c-fos in SCN target cells (Figure S6C).

Second, we asked whether c-fos expression correlates with CTB$^+$ regenerating axons' distribution in the SCN. We performed an automatic detection of c-fos$^+$ and CTB$^+$ points combined with spatial point pattern analysis.[43] We then plotted the density maps of c-fos and CTB across reinnervated SCN sections. The distribution of distances from CTB$^+$ points to c-fos$^+$ points shows that c-fos activation clusters where CTB$^+$ regenerating fibers enter the SCN (Figures S7A and S7B). This is the case in the intact condition, with a detection of both types of events in the SCN core region (Figure S7A), consistent with the fact that, during development, RGC axons enter the SCN ventrally[44] and that connections are more clustered in the SCN core. In the regenerative condition, c-fos is activated mostly in the SCN shell region, and this activation coincides with the dorsal entry point of CTB$^+$ regenerating fibers in the SCN (Figure S7B). Comparison of c-fos$^+$ distributions shows that c-fos is more activated in the SCN core in the intact condition, while during regeneration c-fos is more activated in the shell (Figure S7C). Altogether, these results support that the newly formed retinorecipient circuit triggers functional neuronal activation in the SCN.

## Slit/Robo signaling modulation leads to behavioral recovery of the circadian period

Finally, we asked whether this neuronal circuit could restore function. We took advantage of the SCN role as the master

(yellow) and is adjacent to the post-synaptic compartment marker PSD95 (magenta). Right: resliced view, corresponding to the dashed line in center panel, showing the synapse formed by the CTB$^+$ regenerative fiber. Profile of intensity along the white arrow.
(B) Principle of monosynaptic backtracing.
(C) Schematic of SCN rabies (RVΔG-GFP) injection and detection in input RGC in the retina.
(D) *In situ* hybridization showing *Vip* expression in WT SCN in intact condition and at 28 dpc.
(E) Validation of pVIP-Cre in Rosa26-stop$^{fl/fl}$-TdTomato mice, showing TdTomato expression (magenta) in the SCN labeled with anti-VIP antibody (green).
(F) Validation of RVΔG-GFP infection specifically in the SCN.
(G) Whole-mount retina showing RVΔG-GFP expression in input RGC. Corresponding quantification of GFP$^+$ RGC number per retina.
(H) Confocal picture of whole-mount retinas labeled with anti-melanopsin antibody (magenta), showing an example of melanopsin$^+$/RVΔG-GFP$^+$ RGC. Quantification of melanopsin$^+$ RGC subpopulation distribution in RVΔG-GFP$^+$ RGC ($n$ = 68, $N$ = 5 retinas).
See also Figure S5.

Please cite this article in press as: Delpech et al., Axon guidance during mouse central nervous system regeneration is required for specific brain innervation, Developmental Cell (2024), https://doi.org/10.1016/j.devcel.2024.09.005



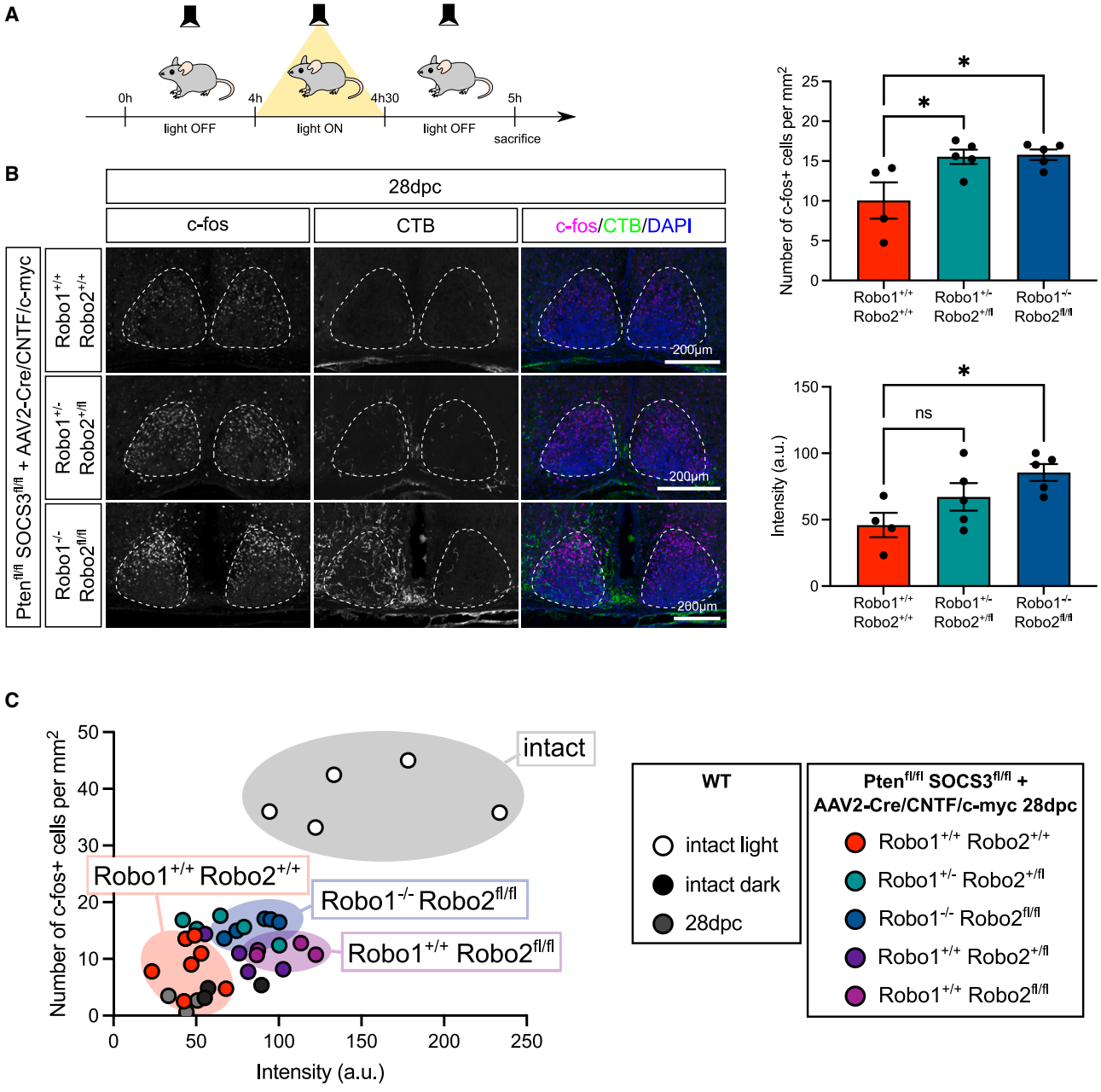


**Figure 6. Guidance of regenerating axons into the SCN results in its reactivation**

(A) Principle of c-fos activation experiment.

(B) Confocal pictures showing SCN expression of c-fos (magenta) in the long-distance regeneration model, in Robo1$^{+/+}$Robo2$^{+/+}$, Robo1$^{+/-}$Robo2$^{+/fl}$ and Robo1$^{-/-}$Robo2$^{fl/fl}$ conditions. Regenerating axons are traced with CTB (green). The white dashed line indicates the SCN. Each picture is representative of $N = 5$ mice. Corresponding quantification of c-fos$^{+}$ cell number per mm$^2$ section in the SCN (top) and of c-fos intensity in c-fos$^{+}$ cells in the SCN (bottom). Data are expressed as mean ± SEM. One-way ANOVA with Dunnett's correction, *$p$ value < 0.05; ns, not significant.

(C) Representation of c-fos$^{+}$ cell number per mm$^2$ section in the SCN versus c-fos intensity.

See also Figures S6 and S7.

regulator of circadian rhythms to assess circuit recovery at the behavioral level. We monitored running wheel activity in a standard 12 h/12 h light/dark cycle, where mice with an intact SCN circuit should have mainly nocturnal activity.[45] To assess behavioral recovery, we compared two groups of animals: Pten$^{fl/fl}$ SOCS3$^{fl/fl}$ + AAV2-Cre/CNTF/c-myc (long-distance regeneration with no SCN reinnervation) and Pten$^{fl/fl}$ SOCS3$^{fl/fl}$ Robo1$^{-/-}$ Robo2$^{fl/fl}$ + AAV2-Cre/CNTF/c-myc (long-distance regeneration with SCN reinnervation and activation) (Figure 7A). At the time of AAV2 injection, both groups show similar circadian rhythms, with a clear activity at night (dark phase) and sleep at day (light phase), and a circadian period indistinguishable from 24 h

Please cite this article in press as: Delpech et al., Axon guidance during mouse central nervous system regeneration is required for specific brain innervation, Developmental Cell (2024), https://doi.org/10.1016/j.devcel.2024.09.005



CellPress
OPEN ACCESS

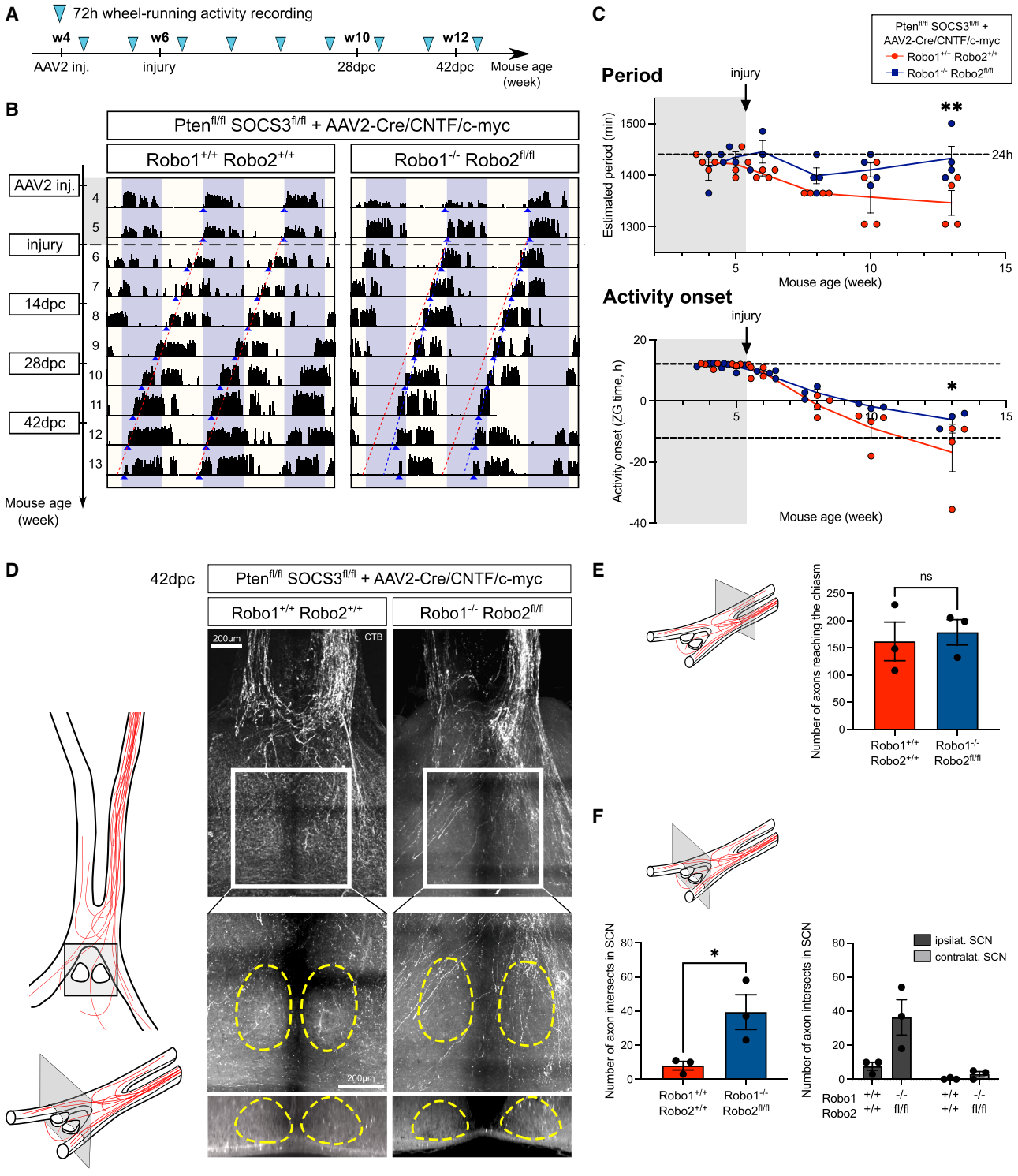


**Figure 7. Guidance of regenerating axons into the SCN results in functional behavioral recovery**

(A) Timeline of wheel-running assay in the long-distance regeneration model.

(B) Representative 72 h actograms recorded every week in relation to environmental light/dark cycle in Pten$^{fl/fl}$ SOCS3$^{fl/fl}$Robo1$^{+/+}$Robo2$^{+/+}$ + AAV2-Cre/CNTF/c-myc and Pten$^{fl/fl}$ SOCS3$^{fl/fl}$Robo1$^{-/-}$Robo2$^{fl/fl}$+AAV2-Cre/CNTF/c-myc. Blue arrowheads point to activity onset. Activity onset slope is shown by the red dashed line in Robo1$^{+/+}$Robo2$^{+/+}$ condition and the blue dashed line in Robo1$^{-/-}$Robo2$^{fl/fl}$ condition.

*(legend continued on next page)*

Please cite this article in press as: Delpech et al., Axon guidance during mouse central nervous system regeneration is required for specific brain innervation, Developmental Cell (2024), https://doi.org/10.1016/j.devcel.2024.09.005



(1,440 min), imposed by the light/dark shift in the environment (Figures 7B and 7C, pre-injury phase).

At the time of bilateral ONC, mice lose visual information relay and adopt a spontaneous circadian rhythm shorter than 24 h (Figures 7B and 7C).This phenomenon is notably described for nocturnal animals kept continuously in the dark (no light stimulation).[45] From this time on, both groups undergo a continuous earlier onset activity due to a shorter intrinsic period, up to 14 dpc. However, we observed that this forwarded onset activity is smaller from 28 dpc in the reinnervated SCN group and is significantly reduced from 42 dpc (Figures 7B and 7C). This is quantified by a period of activity going back 24 h (Figures 7C and S7D). As a control, we performed the same experiment in WT mice with bilateral optic nerve injury and saw no difference with the Pten$^{fl/fl}$ SOCS3$^{fl/fl}$ + AAV2-Cre/CNTF/c-myc group (Figures S7E and S7F).

Despite the light/dark cycle not being fully re-established, these results suggest that the reinnervated SCN group responds to an environmental 24-h light/dark period, unlike the control group that continuously adopts its intrinsic circadian period regardless of environmental visual input. Moreover, we analyzed the number of RGC axons still connected to the SCN and found about 40 regenerating axons inside the SCN at 42 dpc (39 ± 10 intersects in Pten$^{fl/fl}$ SOCS3$^{fl/fl}$ Robo1$^{-/-}$ Robo2$^{fl/fl}$ versus 8 ± 3 intersects in Pten$^{fl/fl}$ SOCS3$^{fl/fl}$) (Figures 7D–7F). We concluded that SCN reinnervation, upon axon guidance, restores a functional circuit. Altogether, our data show that modulation of Robos in the context of long-distance regeneration allows regenerating fibers to connect to SCN target cells and to form a functional neuronal circuit with recovery of circadian activity.

## DISCUSSION

Our study demonstrates that axon guidance is important for circuit formation during axon regeneration in the visual system. Indeed, we show that: (1) the mature SCN expresses repulsive guidance cues that counteract its reinnervation, (2) silencing the repulsive signaling Slit/Robo allows regenerating axons to enter the SCN, and (3) this reinnervation is associated with synapse formation, target cell activation and functional recovery.

Past work on modulation of neuronal intrinsic properties led to long-distance regeneration of some injured axons. However, regenerating axons fail to reinnervate their proper target as they exhibit pathfinding and innervation problems.[8,16,46] Thus, one burning question in the axon regeneration field is: what is mature CNS potential for axon guidance and reinnervation? During development, axon guidance mechanisms are dynamically regulated to shape circuits and precise neuronal connectivity. In the context of CNS repair, resuming correct axon trajectories relies on the fine spatial characterization of the mature CNS environment, which is very different in nature and distribution from the embryonic one.

Previously, guidance cues' expression has been studied at the lesion site. Upon injury, the upregulation of some repulsive guidance factors have been associated with regeneration failure.[46–48] Modulation of these cues was mainly used to assess their role in growth inhibition but never on their guidance properties.[49,50] However, current long-distance regeneration models allow us to re-evaluate their role in axon pathfinding in adults. Recently, we adopted an unbiased proteomics-based approach to establish a map of guidance cues and associated factors in the mature visual system.[15] Surprisingly, mainly repulsive guidance cues are expressed in all areas of the visual system and remain stable upon bilateral ONC. Therefore, triggering axon regrowth is not sufficient to form a neuronal circuit, as regenerating axons face a refractory environment for reinnervation. Yet, manipulation of associated receptors in RGC leads to re-routing axons at the optic chiasm, showing that regenerating axons have the potential to be guided.[15] Here, we focus on SCN/retinal connectivity. Our experiments show a repulsive activity of Slit family members on regenerating axons, similar to embryonic neurons.[34,51] Silencing Slit/Robo signaling provides evidence that axon guidance is determinant for regenerating axons to enter and reconnect their proper brain target.

Several high-throughput data analyses have characterized the injury response and differential resilience of multiple RGC subpopulations.[30,31,42,52] We demonstrated that ipRGC survive and regenerate well in our long-distance model, consistent with previous studies.[6,29,53] Our rabies-tracing experiment shows that ipRGC axons enter and form synapses with SCN neurons upon Slit/Robo silencing. Interestingly, we also found that non-ipRGC subpopulations innervate the SCN, as Slit/Robo signaling was modulated across all RGC subpopulations. As the number of SCN starter neurons expressing the rabies virus is limited, this experiment does not provide an exhaustive quantification. However, our results provide important insight into the identity of RGC connecting the SCN. During development, modalities of circuit formation depend on axon guidance and growth dynamics of each neuronal subpopulation over time. Some RGC project their axon before ipRGC and will not target the SCN, as its innervation window opens at a later stage (e.g., the dLGN [dorsal lateral geniculate nucleus] receives first retinal afferents by E16, while the SCN is connected by P0).[23,54–56] During regeneration, we promoted regrowth of all RGC subpopulations at the same time, losing the temporal regulation that takes place during development. In the future, it will be useful to set up a model of sequential axon growth of different RGC subpopulations. Moreover, mature neuron subpopulations

(C) Top: quantification of estimated period (in minutes) calculated using the Chi-2 periodogram method. Data are expressed as mean ± SEM. Two-way ANOVA with Sidak's correction, $^{**}p$ value = 0.0079. Bottom: quantification of activity onset in zeitgeber hours (hours to beginning of period, light on). Data are expressed as mean ± SEM. Two-way ANOVA with Sidak's correction, $^{*}p$ value = 0.0201.

(D) Confocal picture of whole optic nerves and optic chiasm at 42 dpc in Pten$^{fl/fl}$SOCS3$^{fl/fl}$Robo1$^{+/+}$Robo2$^{+/+}$ + AAV2-Cre/CNTF/c-myc and Pten$^{fl/fl}$SOCS3$^{fl/fl}$Robo1$^{-/-}$Robo2$^{fl/fl}$ + AAV2-Cre/CNTF/c-myc. Regenerating axons are traced using CTB (white). Each picture is representative of $N = 3$ animals. Zoom pictures: the SCN is indicated with the yellow dashed line (maximum projection and XZ orthogonal section panels).

(E) Quantification of the number of axons reaching the chiasm. Data are expressed as mean ± SEM. Unpaired t test; ns, not significant.

(F) Left: quantification of the number of axons entering the SCN. Data are expressed as mean ± SEM. Unpaired t test, $^{*}p$ value = 0.0403; ns, not significant. Right: distribution of axons entering the ipsilateral and contralateral SCN. Data are expressed as mean ± SEM. Unpaired t test; ns, not significant.

See also Figure S7.

Please cite this article in press as: Delpech et al., Axon guidance during mouse central nervous system regeneration is required for specific brain innervation, Developmental Cell (2024), https://doi.org/10.1016/j.devcel.2024.09.005



may actually differ, both in expression of guidance receptors and in the guidance response itself. More generally, the molecular repertoire specifying each RGC subtype's identity may be altered in regenerative conditions, thereby impacting its response to the environment. Therefore, our study deciphers guidance mechanisms as one of the keys to rebuild specific neuronal circuits.

Intriguingly, our results also show that mature SCN innervation is different from the developmental stage. Indeed, most regenerating axons enter the SCN dorsally, consistent with neuronal activation in the SCN shell. During development, ipRGC axons enter the SCN ventrally and connect mostly to the core region.[44] These observations further support the notion that other mechanisms may be at play to control mature SCN reinnervation. Our candidate approach revealed that Sfrp1 and Ephrin-B1 are also expressed in the mature SCN, in addition to all previously identified molecules.[15] It would be interesting to modulate these factors in conjunction with Slit/Robo signaling. Finally, other mechanisms could be at play, such as differential mechanical stiffness in the environment.[26] Our results also uncover unexpected phenotypes, notably an asymmetrical SCN reinnervation with the ipsilateral nucleus preferentially targeted. Interestingly, during development, each SCN is symmetrically connected to both eyes, unlike other retinorecipient brain nuclei. Indeed, almost 50% of ipRGC project bilaterally to each SCN, via branching axons at the optic chiasm.[23] In our regenerative model, it remains unclear whether these mechanisms are still at play. Nonetheless, we observed that both SCN respond symmetrically to photoactivation analyzed by c-fos expression. This may be due to the internal coupling that ensures correct synchronization of both SCN for circadian clock control.[57–59] Alternatively, this may be due to activation of regions neighboring and afferent to the SCN, which in turns activates both nuclei symmetrically. Future work will be needed to characterize the entire SCN neuronal circuit on top of the regenerating RGC projections.

Finally, our work brings evidence for circuit reorganization associated with functional recovery. We demonstrated this feature at multiple levels: synapse formation, post-synaptic neuronal activation, and behavioral recovery. As the SCN is involved in circadian photoentrainment, RGC activation upon light exposure is sufficient to control SCN activity. Our behavioral data show a significant recovery of the visual response to environmental light/dark cycles. This functional recovery does not fully resume the intact circuit, which could be due to mature SCN reinnervation properties. Indeed, the regenerating circuit preferentially activates the SCN shell, in contrast to the intact circuit that has preferential ipRGC projections to the core. Neurons from the shell and the core play different roles in the control of the circadian rhythms and other non-image forming behaviors,[17,60] which may explain why functional recovery is incomplete in our model. Moreover, our results show that only a fraction of ipRGC are able to reach and reinnervate the SCN. This raises the question of how many axons are needed to obtain full functional recovery. Given that other RGC could reconnect the SCN, further investigation is needed to analyze their connectivity to photoreceptors. The results also suggest that these neurons create some compensatory mechanisms contributing to functional recovery. Regarding other brain retinorecipient nuclei, further investigation is needed to decipher whether entry of non-specific axons could also promote functional recovery by compensatory mechanisms. In addition, ipRGC responses are mostly mediated by excitatory glutamatergic signaling,[40,61] but ipRGC were recently shown to also release GABA in the SCN.[62] This non-canonical inhibitory circuit mediates circadian photoentrainment in a light-intensity-dependent manner[62] and remains to be characterized in the case of mature SCN reinnervation, in particular, where SCN-reinnervating ipRGC express GAD markers (GABA synthesis enzymes). Altogether, how the newly formed circuit mediates visual information remains to be fully characterized. Functional reinnervation in the injured CNS through guidance of regenerating axons will set the basis to address this exciting question in the future.

To conclude, our results provide evidence that mature regenerating axons respond to external guidance cues and that modulation of the relevant guidance signaling leads to functional neuronal circuit reconstruction in the mature brain. This study will set the basis of future therapeutic strategies to achieve circuit repair after CNS injury.

## Limitations of the study

Our results show that only a fraction of ipRGC can reach and reinnervate the SCN, raising the question of the axon number needed to obtain full functional recovery. Given that other RGC can reconnect the SCN (based on pan-RGC silencing of Slit/Robo), further investigation is needed to allow ipRGC only to enter the SCN. Moreover, our rabies-tracing experiment underestimates the number of RGC connecting the SCN due to technical limitation. Indeed, we observed toxicity of the rabies viruses for starter cells, impacting the infection rate. However, this experiment provides insight into the identity of RGC connecting the SCN. Finally, the recovery in circadian activity is only partial. This may be partly due to SCN shell activation in regenerative condition (in contrast to core in intact condition), highlighting important differences in reinnervation properties of the mature versus developing SCN.

## RESOURCE AVAILABILITY

### Lead contact

Further information and requests for resources and reagents should be directed to and will be fulfilled by the lead contact, Homaira Nawabi (homaira.nawabi@inserm.fr).

### Materials availability

All unique/stable reagents generated in this study are available from the lead contact upon request without restriction.

### Data and code availability

Data that support the findings of this study are either provided as supplemental information or available from the lead contact upon request. Any additional information required to reanalyze the data reported in this work paper is available from the lead contact upon request.

## ACKNOWLEDGMENTS

We warmly thank Dr. Alexandra Rebsam (Institut de la Vision, Paris, France) and Dr. Julien Falk (INMG, Lyon, France) for their comments and feedback during C.D.'s thesis committee meetings. We warmly thank Dr. Xavier Nicol (Institut de la Vision, Paris, France), Dr. Julien Courchet (INMG, Lyon, France), and Dr. Mireille Albrieux (Grenoble Institute Neuroscience, France) for their comments and feedback during N.V.'s thesis committee meetings. We thank

Charlotte Corrao for *Slit1* ISH plasmid cloning. This work was supported by the Photonic Imaging Center of Grenoble Institute Neuroscience (Univ Grenoble Alpes – Inserm U1216), which is part of the IsdV core facility and certified by the IbiSA label. This work was supported by a grant from ANR (C7H-ANR16C49), from European Research Council (ERC-St17-759089), and NRJ Foundation to H.N. This work was supported by grants from the French National Research Agency in the framework of the "investissements d'Avenir" program (ANR-15-IDEX-02 NeuroCoG) to H.N., S.B., and C.D. and IHU FOReSIGHT (ANR-18-IAHU-01) to A.C. J.S. is supported by Fondation pour la Recherche Médicale (FRM) postdoctoral fellowship (SPF2019090 09106). C.D. is supported by Fondation de France Bourse Berthe Fouassier. N.V. and A.B. are supported by Fondation pour la Recherche Médicale (FRM) thesis fellowship (FDT202204014716 and FDT202304016668).

## AUTHOR CONTRIBUTIONS

Conceptualization and supervision: S.B. and HN. Funding acquisition: H.N and A.C. Methodology: H.N. Investigation, formal analysis, and validation: C.D., J.S., N.V., and A.D. Investigation: A.B. Investigation and resources: E.P., F.A., A.P., B.E., C.G., and A.S. Resources: A.C., V.C., Y.Z., and E.G. Writing – original draft: C.D., J.S., N.V., S.B., and H.N. Writing – review and editing: J.S., N.V., H.N., A.C., and S.B.

## DECLARATION OF INTERESTS

The authors declare no competing interests.

## STAR★METHODS

Detailed methods are provided in the online version of this paper and include the following:

- KEY RESOURCES TABLE
- EXPERIMENTAL MODEL AND STUDY PARTICIPANT DETAILS
- METHOD DETAILS
  - Intravitreal virus injection
  - Optic nerve crush
  - Intracranial injections
  - Neuronal activation assay
  - Adult retina explant cultures
  - Co-culture experiments with SCN explants
  - Co-culture experiments with COS aggregates
  - pVIP-Cre design
  - Monosynaptic tracing
  - Tissue preparation
  - Optic nerve and chiasm clearing
  - Immunostaining
  - In Situ Hybridization
  - Quantitative PCR
  - Imaging
  - Behavioral assay
- QUANTIFICATION AND STATISTICAL ANALYSIS
  - Quantification of guidance defects and SCN reinnervation
  - Quantification of RGC survival
  - Quantification of OPN4-GFP$^{+}$ fibers in the SCN
  - Quantification of Slit2 knockdown in the SCN
  - Quantification of CTB retrograde labeling in the retina
  - Co-culture data analysis
  - Quantification of c-fos-positive cell number and c-fos intensity
  - Spatial point pattern analysis
  - Statistical analysis

## SUPPLEMENTAL INFORMATION

Supplemental information can be found online at https://doi.org/10.1016/j.devcel.2024.09.005.

Received: October 10, 2023
Revised: July 11, 2024
Accepted: September 5, 2024
Published: September 30, 2024

## REFERENCES

1. He, Z., and Jin, Y. (2016). Intrinsic Control of Axon Regeneration. Neuron *90*, 437–451. https://doi.org/10.1016/j.neuron.2016.04.022.
2. Park, K.K., Liu, K., Hu, Y., Smith, P.D., Wang, C., Cai, B., Xu, B., Connolly, L., Kramvis, I., Sahin, M., et al. (2008). Promoting Axon Regeneration in the Adult CNS by Modulation of the PTEN/mTOR Pathway. Science *322*, 963–966. https://doi.org/10.1126/science.1161566.
3. Smith, P.D., Sun, F., Park, K.K., Cai, B., Wang, C., Kuwako, K., Martinez-Carrasco, I., Connolly, L., and He, Z. (2009). SOCS3 deletion promotes optic nerve regeneration in vivo. Neuron *64*, 617–623. https://doi.org/10.1016/j.neuron.2009.11.021.
4. Belin, S., Nawabi, H., Wang, C., Tang, S., Latremoliere, A., Warren, P., Schorle, H., Uncu, C., Woolf, C.J., He, Z., et al. (2015). Injury-induced decline of intrinsic regenerative ability revealed by quantitative proteomics. Neuron *86*, 1000–1014. https://doi.org/10.1016/j.neuron.2015.03.060.
5. Norsworthy, M.W., Bei, F., Kawaguchi, R., Wang, Q., Tran, N.M., Li, Y., Brommer, B., Zhang, Y., Wang, C., Sanes, J.R., et al. (2017). Sox11 Expression Promotes Regeneration of Some Retinal Ganglion Cell Types but Kills Others. Neuron *94*, 1112–1120.e4. https://doi.org/10.1016/j.neuron.2017.05.035.
6. Lim, J.-H.A., Stafford, B.K., Nguyen, P.L., Lien, B.V., Wang, C., Zukor, K., He, Z., and Huberman, A.D. (2016). Neural activity promotes long-distance, target-specific regeneration of adult retinal axons. Nat. Neurosci. *19*, 1073–1084. https://doi.org/10.1038/nn.4340.
7. Sun, F., Park, K.K., Belin, S., Wang, D., Lu, T., Chen, G., Zhang, K., Yeung, C., Feng, G., Yankner, B.A., et al. (2011). Sustained axon regeneration induced by co-deletion of PTEN and SOCS3. Nature *480*, 372–375. https://doi.org/10.1038/nature10594.
8. Crair, M.C., and Mason, C.A. (2016). Reconnecting Eye to Brain. J. Neurosci. *36*, 10707–10722. https://doi.org/10.1523/JNEUROSCI.1711-16.2016.
9. Luo, X., Salgueiro, Y., Beckerman, S.R., Lemmon, V.P., Tsoulfas, P., and Park, K.K. (2013). Three-dimensional evaluation of retinal ganglion cell axon regeneration and pathfinding in whole mouse tissue after injury. Exp. Neurol. *247*, 653–662. https://doi.org/10.1016/j.expneurol.2013.03.001.
10. Pernet, V., Joly, S., Dalkara, D., Jordi, N., Schwarz, O., Christ, F., Schaffer, D.V., Flannery, J.G., and Schwab, M.E. (2013). Long-distance axonal regeneration induced by CNTF gene transfer is impaired by axonal misguidance in the injured adult optic nerve. Neurobiol. Dis. *51*, 202–213. https://doi.org/10.1016/j.nbd.2012.11.011.
11. Pernet, V., Joly, S., Jordi, N., Dalkara, D., Guzik-Kornacka, A., Flannery, J.G., and Schwab, M.E. (2013). Misguidance and modulation of axonal regeneration by Stat3 and Rho/ROCK signaling in the transparent optic nerve. Cell Death Dis. *4*, e734. https://doi.org/10.1038/cddis.2013.266.
12. Wang, X.-W., Yang, S.-G., Zhang, C., Hu, M.-W., Qian, J., Ma, J.-J., Zhang, Y., Yang, B.-B., Weng, Y.-L., Ming, G.-L., et al. (2020). Knocking Out Non-muscle Myosin II in Retinal Ganglion Cells Promotes Long-Distance Optic Nerve Regeneration. Cell Rep. *31*, 107537. https://doi.org/10.1016/j.celrep.2020.107537.
13. Wang, Z., Reynolds, A., Kirry, A., Nienhaus, C., and Blackmore, M.G. (2015). Overexpression of Sox11 Promotes Corticospinal Tract Regeneration after Spinal Injury While Interfering with Functional Recovery. J. Neurosci. *35*, 3139–3145. https://doi.org/10.1523/JNEUROSCI.2832-14.2015.
14. Stoeckli, E.T. (2018). Understanding axon guidance: are we nearly there yet? Development *145*, dev151415. https://doi.org/10.1242/dev.151415.
15. Vilallongue, N., Schaeffer, J., Hesse, A.-M., Delpech, C., Blot, B., Paccard, A., Plissonnier, E., Excoffier, B., Couté, Y., Belin, S., et al. (2022). Guidance

landscapes unveiled by quantitative proteomics to control reinnervation in adult visual system. Nat. Commun. *13*, 6040. https://doi.org/10.1038/s41467-022-33799-4.

16. Schaeffer, J., Vilallongue, N., Belin, S., and Nawabi, H. (2023). Axon guidance in regeneration of the mature central nervous system. Neural Regen. Res. *18*, 2665–2666. https://doi.org/10.4103/1673-5374.373663.
17. Patton, A.P., and Hastings, M.H. (2018). The suprachiasmatic nucleus. Curr. Biol. *28*, R816–R822. https://doi.org/10.1016/j.cub.2018.06.052.
18. Mason, C., and Slavi, N. (2020). Retinal Ganglion Cell Axon Wiring Establishing the Binocular Circuit. Annu. Rev. Vis. Sci. *6*, 215–236. https://doi.org/10.1146/annurev-vision-091517-034306.
19. Baver, S.B., Pickard, G.E., Sollars, P.J., and Pickard, G.E. (2008). Two types of melanopsin retinal ganglion cell differentially innervate the hypothalamic suprachiasmatic nucleus and the olivary pretectal nucleus. Eur. J. Neurosci. *27*, 1763–1770. https://doi.org/10.1111/j.1460-9568.2008.06149.x.
20. Güler, A.D., Ecker, J.L., Lall, G.S., Haq, S., Altimus, C.M., Liao, H.-W., Barnard, A.R., Cahill, H., Badea, T.C., Zhao, H., et al. (2008). Melanopsin cells are the principal conduits for rod–cone input to non-image-forming vision. Nature *453*, 102–105. https://doi.org/10.1038/nature06829.
21. Berson, D.M., Castrucci, A.M., and Provencio, I. (2010). Morphology and mosaics of melanopsin-expressing retinal ganglion cell types in mice. J. Comp. Neurol. *518*, 2405–2422. https://doi.org/10.1002/cne.22381.
22. Hattar, S., Kumar, M., Park, A., Tong, P., Tung, J., Yau, K.-W., and Berson, D.M. (2006). Central projections of melanopsin-expressing retinal ganglion cells in the mouse. J. Comp. Neurol. *497*, 326–349. https://doi.org/10.1002/cne.20970.
23. Fernandez, D.C., Chang, Y.-T., Hattar, S., and Chen, S.-K. (2016). Architecture of retinal projections to the central circadian pacemaker. Proc. Natl. Acad. Sci. USA *113*, 6047–6052. https://doi.org/10.1073/pnas.1523629113.
24. Chaudhry, N., and Filbin, M.T. (2007). Myelin—Associated Inhibitory Signaling and Strategies to Overcome Inhibition. J. Cereb. Blood Flow Metab. *27*, 1096–1107. https://doi.org/10.1038/sj.jcbfm.9600407.
25. Silver, J., Schwab, M.E., and Popovich, P.G. (2014). Central Nervous System Regenerative Failure: Role of Oligodendrocytes, Astrocytes, and Microglia. Cold Spring Harb. Perspect. Biol. *7*, a020602. https://doi.org/10.1101/cshperspect.a020602.
26. Franze, K., Janmey, P.A., and Guck, J. (2013). Mechanics in Neuronal Development and Repair. Annu. Rev. Biomed. Eng. *15*, 227–251. https://doi.org/10.1146/annurev-bioeng-071811-150045.
27. Hattar, S., Liao, H.W., Takao, M., Berson, D.M., and Yau, K.W. (2002). Melanopsin-Containing Retinal Ganglion Cells: Architecture, Projections, and Intrinsic Photosensitivity. Science *295*, 1065–1070. https://doi.org/10.1126/science.1069609.
28. Berson, D.M., Dunn, F.A., and Takao, M. (2002). Phototransduction by Retinal Ganglion Cells That Set the Circadian Clock. Science *295*, 1070–1073. https://doi.org/10.1126/science.1067262.
29. Bray, E.R., Yungher, B.J., Levay, K., Ribeiro, M., Dvoryanchikov, G., Ayupe, A.C., Thakor, K., Marks, V., Randolph, M., Danzi, M.C., et al. (2019). Thrombospondin-1 Mediates Axon Regeneration in Retinal Ganglion Cells. Neuron *103*, 642–657.e7. https://doi.org/10.1016/j.neuron.2019.05.044.
30. Duan, X., Qiao, M., Bei, F., Kim, I.-J., He, Z., and Sanes, J.R. (2015). Subtype-Specific Regeneration of Retinal Ganglion Cells following Axotomy: Effects of Osteopontin and mTOR Signaling. Neuron *85*, 1244–1256. https://doi.org/10.1016/j.neuron.2015.02.017.
31. Tran, N.M., Shekhar, K., Whitney, I.E., Jacobi, A., Benhar, I., Hong, G., Yan, W., Adiconis, X., Arnold, M.E., Lee, J.M., et al. (2019). Single-Cell Profiles of Retinal Ganglion Cells Differing in Resilience to Injury Reveal Neuroprotective Genes. Neuron *104*, 1039–1055.e12. https://doi.org/10.1016/j.neuron.2019.11.006.
32. Schmidt, T.M., Taniguchi, K., and Kofuji, P. (2008). Intrinsic and Extrinsic Light Responses in Melanopsin-Expressing Ganglion Cells During Mouse Development. J. Neurophysiol. *100*, 371–384. https://doi.org/10.1152/jn.00062.2008.
33. Prieur, D.S., and Rebsam, A. (2017). Retinal axon guidance at the midline: Chiasmatic misrouting and consequences. Dev. Neurobiol. *77*, 844–860. https://doi.org/10.1002/dneu.22473.
34. Brose, K., Bland, K.S., Wang, K.H., Arnott, D., Henzel, W., Goodman, C.S., Tessier-Lavigne, M., and Kidd, T. (1999). Slit Proteins Bind Robo Receptors and Have an Evolutionarily Conserved Role in Repulsive Axon Guidance. Cell *96*, 795–806. https://doi.org/10.1016/S0092-8674(00)80590-5.
35. Plump, A.S., Erskine, L., Sabatier, C., Brose, K., Epstein, C.J., Goodman, C.S., Mason, C.A., and Tessier-Lavigne, M. (2002). Slit1 and Slit2 Cooperate to Prevent Premature Midline Crossing of Retinal Axons in the Mouse Visual System. Neuron *33*, 219–232. https://doi.org/10.1016/S0896-6273(01)00586-4.
36. Schaeffer, J., Delpech, C., Albert, F., Belin, S., and Nawabi, H. (2020). Adult Mouse Retina Explants: From ex vivo to in vivo Model of Central Nervous System Injuries. Front. Mol. Neurosci. *13*, 599948. https://doi.org/10.3389/fnmol.2020.599948.
37. Nguyen-Ba-Charvet, K.T., Plump, A.S., Tessier-Lavigne, M., and Chédotal, A. (2002). Slit1 and Slit2 Proteins Control the Development of the Lateral Olfactory Tract. J. Neurosci. *22*, 5473–5480. https://doi.org/10.1523/JNEUROSCI.22-13-05473.2002.
38. Long, H., Sabatier, C., Ma, L., Plump, A., Yuan, W., Ornitz, D.M., Tamada, A., Murakami, F., Goodman, C.S., and Tessier-Lavigne, M. (2004). Conserved Roles for Slit and Robo Proteins in Midline Commissural Axon Guidance. Neuron *42*, 213–223. https://doi.org/10.1016/S0896-6273(04)00179-5.
39. Davison, C., Bedó, G., and Zolessi, F.R. (2022). Zebrafish Slit2 and Slit3 Act Together to Regulate Retinal Axon Crossing at the Midline. J. Dev. Biol. *10*, 41. https://doi.org/10.3390/jdb10040041.
40. Johnson, J., Fremeau, R.T., Duncan, J.L., Rentería, R.C., Yang, H., Hua, Z., Liu, X., LaVail, M.M., Edwards, R.H., and Copenhagen, D.R. (2007). Vesicular Glutamate Transporter 1 Is Required for Photoreceptor Synaptic Signaling But Not For Intrinsic Visual Functions. J. Neurosci. *27*, 7245–7255. https://doi.org/10.1523/JNEUROSCI.0815-07.2007.
41. Ährlund-Richter, S., Xuan, Y., van Lunteren, J.A., Kim, H., Ortiz, C., Pollak Dorocic, I., Meletis, K., and Carlén, M. (2019). A whole-brain atlas of monosynaptic input targeting four different cell types in the medial prefrontal cortex of the mouse. Nat. Neurosci. *22*, 657–668. https://doi.org/10.1038/s41593-019-0354-y.
42. Jacobi, A., Tran, N.M., Yan, W., Benhar, I., Tian, F., Schaffer, R., He, Z., and Sanes, J.R. (2022). Overlapping transcriptional programs promote survival and axonal regeneration of injured retinal ganglion cells. Neuron *110*, 2625–2645.e7. https://doi.org/10.1016/j.neuron.2022.06.002.
43. Baddeley, A., Rubak, E., and Turner, R. (2015). Spatial Point Patterns: Methodology and Applications with R (Routledge & CRC Press). https://www.routledge.com/Spatial-Point-Patterns-Methodology-and-Applications-with-R/Baddeley-Rubak-Turner/p/book/9781482210200.
44. McNeill, D.S., Sheely, C.J., Ecker, J.L., Badea, T.C., Morhardt, D., Guido, W., and Hattar, S. (2011). Development of melanopsin-based irradiance detecting circuitry. Neural Dev. *6*, 8. https://doi.org/10.1186/1749-8104-6-8.
45. Foster, R.G., Hughes, S., and Peirson, S.N. (2020). Circadian Photoentrainment in Mice and Humans. Biology *9*, 180. https://doi.org/10.3390/biology9070180.
46. Pernet, V., and Schwab, M.E. (2014). Lost in the jungle: new hurdles for optic nerve axon regeneration. Trends Neurosci. *37*, 381–387. https://doi.org/10.1016/j.tins.2014.05.002.
47. Bradbury, E.J., and Burnside, E.R. (2019). Moving beyond the glial scar for spinal cord repair. Nat. Commun. *10*, 3879. https://doi.org/10.1038/s41467-019-11707-7.
48. Silver, J., and Miller, J.H. (2004). Regeneration beyond the glial scar. Nat. Rev. Neurosci. *5*, 146–156. https://doi.org/10.1038/nrn1326.

49. Lee, J.K., Geoffroy, C.G., Chan, A.F., Tolentino, K.E., Crawford, M.J., Leal, M.A., Kang, B., and Zheng, B. (2010). Assessing spinal axon regeneration and sprouting in Nogo-, MAG-, and OMgp-deficient mice. Neuron *66*, 663–670. https://doi.org/10.1016/j.neuron.2010.05.002.

50. Joly, S., Jordi, N., Schwab, M.E., and Pernet, V. (2014). The Ephrin receptor EphA4 restricts axonal sprouting and enhances branching in the injured mouse optic nerve. Eur. J. Neurosci. *40*, 3021–3031. https://doi.org/10.1111/ejn.12677.

51. Kidd, T., Bland, K.S., and Goodman, C.S. (1999). Slit is the midline repellent for the robo receptor in Drosophila. Cell *96*, 785–794. https://doi.org/10.1016/s0092-8674(00)80589-9.

52. Tian, F., Cheng, Y., Zhou, S., Wang, Q., Monavarfeshani, A., Gao, K., Jiang, W., Kawaguchi, R., Wang, Q., Tang, M., et al. (2022). Core transcription programs controlling injury-induced neurodegeneration of retinal ganglion cells. Neuron *110*, 2607–2624.e8. https://doi.org/10.1016/j.neuron.2022.06.003.

53. Li, S., Yang, C., Zhang, L., Gao, X., Wang, X., Liu, W., Wang, Y., Jiang, S., Wong, Y.H., Zhang, Y., et al. (2016). Promoting axon regeneration in the adult CNS by modulation of the melanopsin/GPCR signaling. Proc. Natl. Acad. Sci. USA *113*, 1937–1942. https://doi.org/10.1073/pnas.1523645113.

54. Monavarfeshani, A., Sabbagh, U., and Fox, M.A. (2017). Not a one-trick pony: Diverse connectivity and functions of the rodent lateral geniculate complex. Vis. Neurosci. *34*, E012. https://doi.org/10.1017/S0952523817000098.

55. Prieur, D.S., Francius, C., Gaspar, P., Mason, C.A., and Rebsam, A. (2023). Semaphorin-6D and Plexin-A1 Act in a Non–Cell-Autonomous Manner to Position and Target Retinal Ganglion Cell Axons. J. Neurosci. *43*, 5769–5778. https://doi.org/10.1523/JNEUROSCI.0072-22.2023.

56. Guido, W. (2018). Development, form, and function of the mouse visual thalamus. J. Neurophysiol. *120*, 211–225. https://doi.org/10.1152/jn.00651.2017.

57. Michel, S., Marek, R., vanderLeest, H.T., vanSteensel, M.J., Schwartz, W.J., Colwell, C.S., and Meijer, J.H. (2013). Mechanism of bilateral communication in the suprachiasmatic nucleus. Eur. J. Neurosci. *37*, 964–971. https://doi.org/10.1111/ejn.12109.

58. Abel, J.H., Meeker, K., Granados-Fuentes, D., St John, P.C., Wang, T.J., Bales, B.B., Doyle, F.J., Herzog, E.D., and Petzold, L.R. (2016). Functional network inference of the suprachiasmatic nucleus. Proc. Natl. Acad. Sci. USA *113*, 4512–4517. https://doi.org/10.1073/pnas.1521178113.

59. Leak, R.K., Card, J.P., and Moore, R.Y. (1999). Suprachiasmatic pacemaker organization analyzed by viral transynaptic transport. Brain Res. *819*, 23–32. https://doi.org/10.1016/S0006-8993(98)01317-1.

60. Yan, L., Karatsoreos, I., LeSauter, J., Welsh, D.K., Kay, S., Foley, D., and Silver, R. (2007). Exploring Spatiotemporal Organization of SCN Circuits. Cold Spring Harb. Symp. Quant. Biol. *72*, 527–541. https://doi.org/10.1101/sqb.2007.72.037.

61. Purrier, N., Engeland, W.C., and Kofuji, P. (2014). Mice Deficient of Glutamatergic Signaling from Intrinsically Photosensitive Retinal Ganglion Cells Exhibit Abnormal Circadian Photoentrainment. PLoS One *9*, e111449. https://doi.org/10.1371/journal.pone.0111449.

62. Sonoda, T., Li, J.Y., Hayes, N.W., Chan, J.C., Okabe, Y., Belin, S., Nawabi, H., and Schmidt, T.M. (2020). A noncanonical inhibitory circuit dampens behavioral sensitivity to light. Science *368*, 527–531. https://doi.org/10.1126/science.aay3152.

63. Dominici, C., Rappeneau, Q., Zelina, P., Fouquet, S., and Chédotal, A. (2018). Non-cell autonomous control of precerebellar neuron migration by Slit and Robo proteins. Development *145*, dev150375. https://doi.org/10.1242/dev.150375.

64. Lu, W., van Eerde, A.M., Fan, X., Quintero-Rivera, F., Kulkarni, S., Ferguson, H., Kim, H.-G., Fan, Y., Xi, Q., Li, Q.-G., et al. (2007). Disruption of ROBO2 Is Associated with Urinary Tract Anomalies and Confers Risk of Vesicoureteral Reflux. Am. J. Hum. Genet. *80*, 616–632. https://doi.org/10.1086/512735.

65. Rama, N., Dubrac, A., Mathivet, T., Ní Chárthaigh, R.A., Genet, G., Cristofaro, B., Pibouin-Fragner, L., Ma, L., Eichmann, A., and Chédotal, A. (2015). Slit2 signaling through Robo1 and Robo2 is required for retinal neovascularization. Nat. Med. *21*, 483–491. https://doi.org/10.1038/nm.3849.

66. Nawabi, H., Briançon-Marjollet, A., Clark, C., Sanyas, I., Takamatsu, H., Okuno, T., Kumanogoh, A., Bozon, M., Takeshima, K., Yoshida, Y., et al. (2010). A midline switch of receptor processing regulates commissural axon guidance in vertebrates. Genes Dev. *24*, 396–410. https://doi.org/10.1101/gad.542510.

67. Charoy, C., Nawabi, H., Reynaud, F., Derrington, E., Bozon, M., Wright, K., Falk, J., Helmbacher, F., Kindbeiter, K., and Castellani, V. (2012). gdnf activates midline repulsion by Semaphorin3B via NCAM during commissural axon guidance. Neuron *75*, 1051–1066. https://doi.org/10.1016/j.neuron.2012.08.021.

68. Hahm, S.H., and Eiden, L.E. (1996). Tissue-Specific Expression of the Vasoactive Intestinal Peptide Gene Requires Both an Upstream Tissue Specifier Element and the 5′ Proximal Cyclic AMP-Responsive Element. J. Neurochem. *67*, 1872–1881. https://doi.org/10.1046/j.1471-4159.1996.67051872.x.

69. Dodt, H.-U., Leischner, U., Schierloh, A., Jährling, N., Mauch, C.P., Deininger, K., Deussing, J.M., Eder, M., Zieglgänsberger, W., and Becker, K. (2007). Ultramicroscopy: three-dimensional visualization of neuronal networks in the whole mouse brain. Nat. Methods *4*, 331–336. https://doi.org/10.1038/nmeth1036.

70. Krizo, J.A., and Mintz, E.M. (2014). Sex Differences in Behavioral Circadian Rhythms in Laboratory Rodents. Front. Endocrinol. (Lausanne) *5*, 234. https://doi.org/10.3389/fendo.2014.00234.

71. Rosenfeld, C.S. (2017). Sex-Dependent Differences in Voluntary Physical Activity. J. Neurosci. Res. *95*, 279–290. https://doi.org/10.1002/jnr.23896.

72. Feillet, C., Guérin, S., Lonchampt, M., Dacquet, C., Gustafsson, J.-Å., Delaunay, F., and Teboul, M. (2016). Sexual Dimorphism in Circadian Physiology Is Altered in LXRα Deficient Mice. PLoS One *11*, e0150665. https://doi.org/10.1371/journal.pone.0150665.

73. Schmid, B., Helfrich-Förster, C., and Yoshii, T. (2011). A New ImageJ Plug-in "ActogramJ" for Chronobiological Analyses. J. Biol. Rhythms *26*, 464–467. https://doi.org/10.1177/0748730411414264.

74. Claes, M., and Moons, L. (2022). Retinal Ganglion Cells: Global Number, Density and Vulnerability to Glaucomatous Injury in Common Laboratory Mice. Cells *11*, 2689. https://doi.org/10.3390/cells11172689.

75. Torres-Espín, A., Santos, D., González-Pérez, F., del Valle, J., and Navarro, X. (2014). Neurite-J: An Image-J plug-in for axonal growth analysis in organotypic cultures. J. Neurosci. Methods *236*, 26–39. https://doi.org/10.1016/j.jneumeth.2014.08.005.

76. Bankhead, P., Loughrey, M.B., Fernández, J.A., Dombrowski, Y., McArt, D.G., Dunne, P.D., McQuaid, S., Gray, R.T., Murray, L.J., Coleman, H.G., et al. (2017). QuPath: Open source software for digital pathology image analysis. Sci. Rep. *7*, 16878. https://doi.org/10.1038/s41598-017-17204-5.

Please cite this article in press as: Delpech et al., Axon guidance during mouse central nervous system regeneration is required for specific brain innervation, Developmental Cell (2024), https://doi.org/10.1016/j.devcel.2024.09.005





## STAR★METHODS

### KEY RESOURCES TABLE

| REAGENT or RESOURCE | SOURCE | IDENTIFIER |
|---|---|---|
| **Antibodies** | | |
| Chicken polyclonal anti-GFP antibody | Abcam | Cat# ab13970; RRID: AB_300798 |
| Goat polyclonal anti-VGLUT2 antibody | Abcam | Cat# ab178538; RRID: AB_3661773 |
| Goat anti-CART antibody | R&D Systems | Cat# AF163; RRID: AB_2068569 |
| Goat anti-parvalbumin antibody | Abcam | Cat# ab32895; RRID: AB_777105 |
| Goat anti-osteopontin | R&D Systems | Cat# AF808; RRID: AB_2194992 |
| Guinea polyclonal pig anti-RBPMS antibody | Millipore | Cat# ABN1376; RRID: AB_2687403 |
| Mouse monoclonal anti-tubulin β3 (TUJ1) antibody | Biolegend | Cat# 801202;RRID: AB_10063408 |
| Mouse monoclonal anti-PSD95 antibody | Abcam | Cat# ab2723 ; RRID: AB_303248 |
| Mouse anti-Neurofilament H (NF-H), nonphosphorylated antibody (clone SMI-32) | Biolegend | Cat# 801701; RRID: AB_2564642 |
| Rabbit polyclonal anti-VIP (Vasoactive Intestinal Peptide) antibody | Immunostar | Cat# 20077;RRID: AB_572270 |
| Rabbit monoclonal anti-c-fos antibody | Cell Signaling Technology | Cat# 2250 ; RRID: AB_2247211 |
| Rabbit anti-FOXP2 | Abcam | Cat# ab16046; RRID: AB_2107107 |
| Rabbit polyclonal anti-melanopsin antibody | Abcam | Cat# ab19306; RRID: AB_444842 |
| Rabbit polyclonal anti-Cre recombinase antibody | Biolegend | Cat# 908001; RRID: AB_2565079 |
| Goat polyclonal anti-Robo1 antibody | R&D Systems | Cat# AF1749; RRID: AB_354969 |
| Goat polyclonal anti-Robo2 antibody | Dr Alain Chédotal (Institut de la Vision, Paris, France; MeLiS, University Claude Bernard Lyon 1, Hospices civils de Lyon, Lyon, France); Dominici et al.[63] | N/A |
| Donkey anti-rabbit IgG (H+L) highly cross-absorbed secondary antibody, Alexa Fluor 488 | Thermo Fisher Scientific | Cat# A-21206;RRID: AB_2535792 |
| Donkey anti-rabbit IgG (H+L) highly cross-absorbed secondary antibody, Alexa Fluor 647 | Thermo Fisher Scientific | Cat# A-31573;RRID: AB_2536183 |
| Donkey anti-chicken IgY (IgG) (H+L) antibody, Alexa Fluor 488 | Jackson ImmunoResearch Labs | Cat# 703-545-155; RRID: AB_2340375 |
| Donkey anti-guinea pig IgG (H+L), Alexa Fluor 647 | Jackson ImmunoResearch Labs | Cat# 706-605-148; RRID: AB_2340476 |
| Donkey anti-goat IgG (H+L), Alexa Fluor 488 | Thermo Fisher Scientific | Cat# A11055; RRID: AB_2534102 |
| Donkey anti-mouse IgG (H+L), Alexa Fluor 647 | Thermo Fisher Scientific | Cat# A31571; RRID_162542 |
| Donkey anti-mouse IgG (H+L), Alexa Fluor 568 | Thermo Fisher Scientific | Cat# A10037; RRID: AB_2534013 |
| **Bacterial and virus strains** | | |
| AAV2-Cre | Belin et al.[4] | N/A |
| AAV2-CNTF | Belin et al.[4] | N/A |
| AAV2-c-myc | Belin et al.[4] | N/A |
| AAV2-TVA-RG | Produced using pAAV-DIO-TVA-V5-RG (see Recombinant DNA) | N/A |
| AAV2-pVIP-Cre | This paper | N/A |

(*Continued on next page*)

Please cite this article in press as: Delpech et al., Axon guidance during mouse central nervous system regeneration is required for specific brain innervation, Developmental Cell (2024), https://doi.org/10.1016/j.devcel.2024.09.005



*Continued*

| REAGENT or RESOURCE | SOURCE | IDENTIFIER |
|---|---|---|
| EnvA-RV-ΔG-GFP | Canadian Neurophotonics Platform Viral Vector Core Facility (RRID: SCR_016477) | B19-deltaG-GFP 1437-EnvA |
| **Chemicals, peptides, and recombinant proteins** | | |
| Cholera toxin B subunit (CTB)-Alexa 488 | Thermo Fisher Scientific | Cat# C34775 |
| Cholera toxin B subunit (CTB)-Alexa 555 | Thermo Fisher Scientific | Cat# C22843 |
| Cholera toxin B subunit (CTB)-Alexa 647 | Thermo Fisher Scientific | Cat# C34778 |
| Laminin | Sigma Aldrich | Cat# L2020 |
| Poly-L-Lysine | Sigma Aldrich | Cat# P1399 |
| Collagen I, rat tail | Thermo Fisher Scientific | Cat# A1048301 |
| **Experimental models: Organisms/strains** | | |
| Mouse: Pten$^{fl/fl}$ SOCS3$^{fl/fl}$ | Sun et al.[7]; The Jackson Laboratory | N/A |
| Mouse: OPN4-GFP | STOCK Tg(Opn4-EGFP) ND100Gsat/Mmucd | RRID:MMRRC_033064-UCD |
| Mouse: OPN4-GFP Pten$^{fl/fl}$ SOCS3$^{fl/fl}$ | Schmidt et al.[32]; Sun et al.[7]; The Jackson Laboratory | N/A |
| Mouse: Pten$^{fl/fl}$ SOCS3$^{fl/fl}$ Robo1$^{-/-}$ Robo2$^{fl/fl}$ | Long et al.[38]; Lu et al.[64]; Sun et al.[7]; Dr Alain Chédotal (Institut de la Vision, Paris, France; MeLiS, University Claude Bernard Lyon 1, Hospices civils de Lyon, Lyon, France) | N/A |
| Mouse: Pten$^{fl/fl}$ SOCS3$^{fl/fl}$ Robo1$^{-/-}$ | Long et al.[38]; Lu et al.[64]; Sun et al.[7]; Dr Alain Chédotal (Institut de la Vision, Paris, France; MeLiS, University Claude Bernard Lyon 1, Hospices civils de Lyon, Lyon, France) | N/A |
| Mouse: Pten$^{fl/fl}$ SOCS3$^{fl/fl}$ Robo2$^{fl/fl}$ | Long et al.[38]; Lu et al.[64]; Sun et al.[7]; Dr Alain Chédotal (Institut de la Vision, Paris, France; MeLiS, University Claude Bernard Lyon 1, Hospices civils de Lyon, Lyon, France) | N/A |
| Mouse: OPN4-GFP Pten$^{fl/fl}$ SOCS3$^{fl/fl}$ Robo1$^{-/-}$ Robo2$^{fl/fl}$ | Schmidt et al.[32]; Sun et al.[7]; The Jackson Laboratory; Long et al.[38]; Lu et al.[64]; Dr Alain Chédotal (Institut de la Vision, Paris, France; MeLiS, University Claude Bernard Lyon 1, Hospices civils de Lyon, Lyon, France) | N/A |
| Mouse: Slit1$^{-/-}$ | Dr Alain Chédotal (Institut de la Vision, Paris, France; MeLiS, University Claude Bernard Lyon 1, Hospices civils de Lyon, Lyon, France) | N/A |
| Mouse: Slit2$^{fl/fl}$ | Rama et al.,[65]; Dr Alain Chédotal (Institut de la Vision, Paris, France; MeLiS, University Claude Bernard Lyon 1, Hospices civils de Lyon, Lyon, France) | N/A |
| Mouse: Slit1$^{-/-}$ Slit2$^{fl/fl}$ | Dr Alain Chédotal (Institut de la Vision, Paris, France; MeLiS, University Claude Bernard Lyon 1, Hospices civils de Lyon, Lyon, France) | N/A |
| Mouse: Slit3$^{-/-}$ | Dr Alain Chédotal (Institut de la Vision, Paris, France; MeLiS, University Claude Bernard Lyon 1, Hospices civils de Lyon, Lyon, France) | N/A |
| Mouse: Rosa26-stop$^{fl/fl}$-TdTomato | The Jackson Laboratory | RRID:IMSR_JAX:007914 |
| **Oligonucleotides** | | |
| Primer ISH: Plexin-A1 Forward; 5'-CCCCCACTGTGGCTGGTGTG-3' | This paper | N/A |
| Primer ISH: Plexin-A1 Reverse; 5'-GAAAGGCGCAGTCAGCCGCA-3' | This paper | N/A |

(*Continued on next page*)

Please cite this article in press as: Delpech et al., Axon guidance during mouse central nervous system regeneration is required for specific brain innervation, Developmental Cell (2024), https://doi.org/10.1016/j.devcel.2024.09.005





*Continued*

| REAGENT or RESOURCE | SOURCE | IDENTIFIER |
|---|---|---|
| Primer ISH: Robo1 Forward; 5'-AGCAGTGGATGGCACTTTAA-3' | This paper | N/A |
| Primer ISH: Robo1 Reverse; 5'-GGAAAAGGTAAATGGCGTTA-3' | This paper | N/A |
| Primer ISH: Robo2 Forward; 5'-CTTTTCCCGAATCAACCTCA-3' | This paper | N/A |
| Primer ISH: Robo2 Reverse; 5'-GGGAGGTCATTCATATCATA-3' | This paper | N/A |
| Primer ISH: Sema6D Forward; 5'-TTCCTCCATGTGTGTCCTGT-3' | This paper | N/A |
| Primer ISH: Sema6D Reverse; 5'-GTTGGGTAAATGACTGGGTGATGT-3' | This paper | N/A |
| Primer ISH: Sfrp1 Forward; 5'-GGACCTGAGGCTGTGCCACA-3' | This paper | N/A |
| Primer ISH: Sfrp1 Reverse; 5'-TCTTCTTGGGGACAATCTTC-3' | This paper | N/A |
| Primer ISH: Sfrp2 Forward; 5'-GCCCAACCTGCTGGGCCACG-3' | This paper | N/A |
| Primer ISH: Sfrp2 Reverse; 5'-CGCCGTTCAGCTTGTAAATG-3' | This paper | N/A |
| Primer ISH: Slit1 Forward; 5'-CACTGGGTTGTTTAAGAAGC-3' | This paper | N/A |
| Primer ISH: Slit1 Reverse; 5'-CCTGGCCTTCCTCACACCTG-3' | This paper | N/A |
| Primer ISH: Slit2 Forward; 5'-CCTGCCAGCATGACTCCAAG-3' | This paper | N/A |
| Primer ISH: Slit2 Reverse; 5'-TCTATAGAGTTCCACGGCAA-3' | This paper | N/A |
| Primer ISH: VEGF-A Forward; 5'-GCAGCGACAAGGCAGACTA-3' | This paper | N/A |
| Primer ISH: VEGF-A Reverse; 5'-GCTAGCACTTCTCCCAGCTC-3' | This paper | N/A |
| Primer qPCR: Slit1 Forward; 5'-AGGTGCAAAAGGGCGAAT-3' | This paper | N/A |
| Primer qPCR: Slit1 Reverse; 5'-CGAGAGGGTACAGGCAGGT-3' | This paper | N/A |
| Primer qPCR: Slit2 Forward; 5'-CGGGGACAGCTGTGATAGAG-3' | This paper | N/A |
| Primer qPCR: Slit2 Reverse; 5'-CCAAGCGAGATACTTTCTTAGTTGT-3' | This paper | N/A |
| Primer qPCR: Slit3 Forward; 5'-gccacctcagtgagaacctc-3' | This paper | N/A |
| Primer qPCR: Slit3 Reverse; 5'-tgtccctcaaagcccaga-3' | This paper | N/A |
| Primer qPCR: Gapdh Forward; 5'-GCATGGCCTTCCGTGTTC-3', | This paper | N/A |
| Primer qPCR: Gapdh Reverse; 5'-TGTCATCATACTTGGCAGGTTTCT-3' | This paper | N/A |
| **Recombinant DNA** | | |
| Plasmid ISH: Ephrin-B1 | Dr Valérie Castellani (MeLiS, University Claude Bernard Lyon 1, Lyon, France) | N/A |
| Plasmid ISH: Netrin1 | Dr Valérie Castellani (MeLiS, University Claude Bernard Lyon 1, Lyon, France); Nawabi et al.[66] | N/A |

(*Continued on next page*)

*Continued*

| REAGENT or RESOURCE | SOURCE | IDENTIFIER |
|---|---|---|
| Plasmid ISH: NrCAM | Dr Valérie Castellani (MeLiS, University Claude Bernard Lyon 1, Lyon, France); Nawabi et al.[66] | N/A |
| Plasmid ISH: Shh | Dr Valérie Castellani (MeLiS, University Claude Bernard Lyon 1, Lyon, France); Charoy et al.[67] | N/A |
| Plasmid ISH: Slit3 | Dr Alain Chédotal (Institut de la Vision, Paris, France; MeLiS, University Claude Bernard Lyon 1, Hospices civils de Lyon, Lyon, France) | N/A |
| Plasmid pAAV-pVIP-Cre | This paper | N/A |
| Plasmid pAAV-DIO-TVA-V5-RG | Kind gift from Dr Marie Carlén; Ährlund-Richter et al.[41] | Addgene #119743; RRID:Addgene_119743 |
| Software and algorithms | | |
| Zen | Zeiss | N/A |
| Fiji | Image J | N/A |
| IMARIS v.9.6 | Bitplane | N/A |
| GraphPad Prism 9 | GraphPad software | N/A |
| Fusion | Andor | N/A |

## EXPERIMENTAL MODEL AND STUDY PARTICIPANT DETAILS

All animal care and procedures have been approved by the Ethics Committee of the Grenoble Institute of Neuroscience (project number 201612161701775) and by the French Ministry of Research (project number APAFIS#9145- 201612161701775v3) in accordance with French and European guidelines. All animal care and procedures were performed in compliance with the Grenoble Institute of Neuroscience-U1216, French and European guidelines. We used Pten$^{fl/fl}$ SOCS3$^{fl/fl}$, OPN4-GFP Pten$^{fl/fl}$ SOCS3$^{fl/fl}$, Pten$^{fl/fl}$ SOCS3$^{fl/fl}$ Robo1$^{-/-}$ Robo2$^{fl/fl}$, Pten$^{fl/fl}$ SOCS3$^{fl/fl}$ Robo1$^{-/-}$, Pten$^{fl/fl}$ SOCS3$^{fl/fl}$ Robo2$^{fl/fl}$, Slit1$^{-/-}$,[65] Slit2$^{fl/fl}$,[65] Slit1$^{-/-}$, Slit2$^{fl/fl}$,[65] and Slit3$^{-/-}$ mice in this study, regardless of their sex (except for behavior assay where only females were used) and aged at least 3 weeks. To obtain OPN4-GFP Pten$^{fl/fl}$ SOCS3$^{fl/fl}$ mice, we crossed OPN4-GFP mice[32] with Pten$^{fl/fl}$ SOCS3$^{fl/fl}$.[7] To obtain Pten$^{fl/fl}$ SOCS3$^{fl/fl}$ Robo1$^{-/-}$ Robo2$^{fl/fl}$ mice, we crossed Pten$^{fl/fl}$ SOCS3$^{fl/fl}$ mice with Pten$^{fl/fl}$ Robo1$^{-/-}$ Robo2$^{fl/fl}$ mice.[38,64] To obtain OPN4-GFP Pten$^{fl/fl}$ SOCS3$^{fl/fl}$ Robo1$^{-/-}$ Robo2$^{fl/fl}$ mice, we crossed OPN4-GFP mice with Pten$^{fl/fl}$ SOCS3$^{fl/fl}$ Robo1$^{-/-}$ Robo2$^{fl/fl}$ mice. Mice were housed in standard housing conditions with a 12 h light/dark cycle. When possible, animals were housed in groups of 2–5 per cage. Animals were fed and watered ad libitum. Before each surgery, all animals were anesthetized with an intraperitoneal injection of ketamine (100 mg/kg, Clorkétam 1000, Vetoquinol) and xylasine (10 mg/kg, Rompun 2%, BAYER).

## METHOD DETAILS

### Intravitreal virus injection

Intravitreal injections were performed as described.[36] The eyelid of the eye was pinched with a mini bulldog serrefines clamp (Fine Science Tools) to bring out the eyeball and expose the posterior part of the eye. Using a Hamilton syringe (Hamilton) connected to a glass micropipette (Sutter Instruments), the posterior part of the eye located just behind the ora serrata was punctured with an angle of 45° to avoid damaging the lens. About 2μL of vitreous humor was taken out before injecting 1μL of adeno-associated virus type 2 (AAV2), concentrated with at least $10^{11}$ viral particles per mL. Viral vectors used in this study are AAV2-Cre, AAV2-CNTF and AAV2-c-myc. 1 day before sacrifice, animals received an intravitreal injection of 1μL of CTB at 1μg/μL (ThermoFisher Scientific). Mice with eye inflammation, damage or atrophies were excluded from further experiments.

### Optic nerve crush

2 weeks after the AAV2 intravitreal injections, optic nerve crush was performed. The connective tissue above the eye was cut using scissors (Fine Science Tools). Forceps (Fine Science Tools, 11251-20) were then placed between the 2 arteries located behind the eyeball in order to expose the optic nerve. Using a second pair of forceps, the optic nerve was pinched for 5 seconds at 1-2 mm behind the eyeball. Animals with excessive bleeding were excluded from further experiments.

### Intracranial injections

10-week-old Pten$^{fl/fl}$ SOCS3$^{fl/fl}$, Slit2$^{fl/fl}$ or Slit1$^{-/-}$ Slit2$^{fl/fl}$ mice were anesthetized and installed on a stereotaxic frame. The skin was cut letting the skull visible. Using the canula, the bregma was defined as the origin of axes. After verifying flat skull positioning, one

Please cite this article in press as: Delpech et al., Axon guidance during mouse central nervous system regeneration is required for specific brain innervation, Developmental Cell (2024), https://doi.org/10.1016/j.devcel.2024.09.005





hole was performed using a dental bur at A/P: +1mm, M/L: +0.1mm, D/V: -6mm (for SCN injection) and -6.5mm (for chiasm injection). 1μL of virus (AAV2-Cre for co-culture experiment, Slit2$^{fl/fl}$ or Slit1$^{-/-}$ Slit2$^{fl/fl}$ mice) or CTB (for retrograde labeling, Pten$^{fl/fl}$ SOCS3$^{fl/fl}$) was injected using a syringe pump (0.5μL/min). After injection, the skin was sutured and animals were sacrificed 2 weeks later.

### Neuronal activation assay

To study SCN neuron activation upon light exposure, 4h after the dark cycle start, we exposed mice for 30min to light before going back 30min to dark (4h dark - 30min light - 30min dark; this scheme is called 4-30-30). We designed 6 mice groups. Group 1 (positive control): WT intact mice with 4-30-30 condition. Group 2 (negative control): WT intact mice kept in the dark. Group 3: WT mice with bilateral optic nerve lesion in 4-30-30 condition. Group 4: Pten$^{fl/fl}$ SOCS3$^{fl/fl}$ Robo1$^{+/+}$ Robo2$^{+/+}$ mice in 4-30-30 condition. Group 5: Pten$^{fl/fl}$ SOCS3$^{fl/fl}$ Robo1$^{+/-}$ Robo2$^{+/fl}$ mice in 4-30-30 condition. Group 6: Pten$^{fl/fl}$ SOCS3$^{fl/fl}$ Robo1$^{-/-}$ Robo2$^{fl/fl}$ in 4-30-30 condition. Groups 4 to 6 received a unilateral injection of AAV2-Cre/CNTF/c-myc as described above, then a bilateral ONC two weeks later. Two days before sacrifice, groups 4 to 6 received an intravitreal injection of CTB to control for complete injuries. For groups 4-6, neuronal activation assay was performed at 28dpc. After 4-30-30 conditioning, mice were sacrificed and perfused in the dark. Brains were dissected out and sectioned into 40μm thick-section. Immunofluorescence with anti-c-fos antibody was performed.

### Adult retina explant cultures

Adult retina explant cultures were performed as described.[36] Both eyes of 4-week-old Pten$^{fl/fl}$ SOCS3$^{fl/fl}$ mice were injected with AAV2-Cre + AAV2-CNTF on day 0, then AAV2-c-myc on day 1. Two weeks later, mice were sacrificed by cervical dislocation and retinas were dissected out in Hibernate-A and cut into small pieces (about 500μm in diameter, as described[36]). Explants were laid on glass coverslips previously coated with 0.5mg/mL poly-L-lysine overnight at room temperature, then with 20μg/mL laminin for 2h at room temperature, then with a thin layer of coating medium (4mg/mL methylcellulose, 2% B27 (ThermoFisher Scientific), 1% L-Glutamine (Corning) in Hibernate-A). Explants were cultured for 7 to 10 days before fixation and immunofluorescence.

### Co-culture experiments with SCN explants

Two weeks after intracranial injection of Slit2$^{fl/fl}$ or Slit1$^{-/-}$ Slit2$^{fl/fl}$ mice, animals were sacrificed by cervical dislocation. Fresh brains were sectioned using a vibratome (300μm thick sections). The two SCN were microdissected out, each constituting one SCN explant. Glass coverslips used for the co-cultures were previously coated with 0.5mg/mL poly-L-lysine for 1h at 37°C. After washes and air-dry, a thin layer of collagen matrix was applied on each coverslip (500μL of 3mg/mL collagen I (from rat tail, Thermo Scientific), 20μL of 1mg/mL laminin (Sigma-Aldrich), 12.5μL of 1N NaOH, 100μL of PBS 10X (Euromedex) and 367.5μL of Neurobasal-A) and left to polymerize at 37°C for 20 min. In parallel, retina from Pten$^{fl/fl}$ SOCS3$^{fl/fl}$ previously injected with AAV2-Cre/CNTF/c-myc were dissected out and prepared for explants. A retina explant and a SCN explant were laid onto the coated coverslip and a 60μL drop of the collagen mix was applied. Co-cultures were placed at 37°C for few minutes before adding the culture medium: 2% B27, 1% L-Glutamine, 1% Penicillin/Streptomycin (ThermoFisher Scientific) in Neurobasal-A (ThermoFisher Scientific). Co-cultures were incubated at 37°C with 5% $CO_2$ for 10 days before fixation and immunofluorescence.

### Co-culture experiments with COS aggregates

#### *COS cells transfection*

COS cells were seeded in 6-well plate in complete DMEM medium (Fisher Scientific, 12077549; supplemented with 10% of fetal bovine serum (EuroBio Scientific, CVFSVF0001) and 1% Penicillin-Streptomycin (Thermo Fisher Scientific, 15140122)), and when 70 to 90% of confluence were reached, they were transfected with plasmids expressing Slit1, Slit2 or Slit3 using lipofectamine (Lipofectamine 3000 transfection kit, Invitrogen, L3000-015). Briefly, for each well, 3.75μl of lipofectamine was vortexed with 125μl of Optimem (Fisher Scientific, 11564506); in a separate tube, 5μl of P3000 lipofectamine reagent were vortexed with 2.5μg of DNA and 125μl of Optimem. After mixing and vortexing both tubes, they were incubated for 15min at room temperature. 250μl of transfection mix was added to each well and cells were incubated at 37°C for 3 days.

#### *Agarose drop production*

Three days after the transfection, complete DMEM medium was removed and 500μl of 0.25% trypsin 1X (Corning, 25-050-CI) was added per well, for 10min at 37°C. Reaction was stopped by supplementing with 1ml of DMEM medium and cells were retrieved in a 1.5ml tube. After a 10 min centrifugation at 100g at room temperature, supernatant was removed and 10μl of complete DMEM medium was added. Then, 30μl of 2% agarose (Ultrapure LMP agarose, Invitrogen, 16520-050) was mixed to the cells and drops were realized on a new 6-well plate. When drops were solidified, they are put in culture with adult retina explants.

### pVIP-Cre design

The SCN-specific Cre expression was performed by cloning the Cre recombinase cloned under a minimal VIP promoter, designed according to Hahm and Eiden[68] and adapted using the mouse genome, leading to the following sequence: 5'-CAGTAGATAGCA TAAATTTCAAGCCAGCCACTAGACATCACTGTTTCTCATTTCACCCATCAGTAAACCTAGAAGAACCCTGGGTTAAAGACTGACTACT GAGAATGTGGGCTCATCACAGCTAAGTAAAGATTAAAGCATTGCACATCCAGCTAAGTACTTTTCTTTTTTTAAAAAAGAGTTCATTT CCTCTCTCTTGAACTTGTTTGCTATAAATGTATATAAATCAGGCATGATGACAATTTAATAAGAACTTCAAGACCTGTTCATCCCATGG GATCACTACTGTGACGTCTTTCGGGGAGCCTTCTGATTGCTCAGCCCGAAGCACAAGCCCTATAAAATGAGAGACTTTGAGA-3′. SCN specificity was monitored using Rosa26-stop$^{fl/fl}$-TdTomato mice (see Figure 5D).

Please cite this article in press as: Delpech et al., Axon guidance during mouse central nervous system regeneration is required for specific brain innervation, Developmental Cell (2024), https://doi.org/10.1016/j.devcel.2024.09.005



## Monosynaptic tracing

4 week-old Pten$^{fl/fl}$ SOCS3$^{fl/fl}$ Robo1$^{-/-}$ Robo2$^{fl/fl}$ mice were intravitreally injected with AAV2-Cre, AAV2-CNTF and AAV2-c-myc (as previously described, in order to promote axon regeneration and SCN reinnervation). 2 weeks after, bilateral optic nerve crush was performed as previously described. 3 weeks later, intracranial injection of pVIP-Cre and TVA-V5-RG protein (1:1, 1μl total) was done in the suprachiasmatic nucleus as previously described. One week later, using the same procedure, 1μl of pseudotyped rabies virus EnvA-ΔG-RV-GFP virus (B19-deltaG-GFP 1437-EnvA from Canadian Neurophotonics Platform Viral Vector Core Facility (RRID:SCR_016477), concentration for injection: 2.2x10$^7$ TU/mL) was injected at the same injection site. 6 days later, animals received an intravitreal injection of 1μL of CTB at 1μg/μL (ThermoFisher Scientific) (AlexaFluor-555) in each eye to assess optic nerve crush, regeneration and SCN reinnervation. The day after, animals were perfused as described below. pAAV-DIO-TVA-V5-RG[41] was a gift from Marie Carlén (Addgene plasmid #119743).

## Tissue preparation

At 28dpc animals were anesthetized with ketamine (100 mg/kg) and xylasine (10 mg/kg) and then intracardially perfused with ice-cold PBS and ice-cold 4% paraformaldehyde dissolved in PBS (PFA) (Electron Microscopy Sciences). Brains, optic nerves and eyes were dissected and post-fixed in 4% PFA overnight at 4°C. Brains and eyes were dehydrated in 30% sucrose (Sigma-Aldrich) for 2 days at 4°C before embedding in OCT tissue freezing medium (MM-France) and stored at -80°C. Using cryostat sectioning, 20μm coronal brain, 14μm eyes and 14μm optic nerve sections were performed. Sections were collected on SuperFrost slides (ThermoFisher Scientific) and stored at -20°C until further use.

## Optic nerve and chiasm clearing

Optic nerves, chiasm and/or SCN were clarified as described.[69] First, samples were post-fixed in 4% PFA overnight at 4°C. If necessary, samples were first permeabilized in PBS 0.5% Triton X-100 for 2h at room temperature and incubated in 10μg/mL DAPI (Sigma-Aldrich-Merck, D9542) for 30min, then washed several times in PBS 0.5% Triton X-100. Alternatively, samples were permeabilized, blocked in PBS 0.5% Triton X-100 5% donkey serum and stained for anti-VIP (1:400, Immunostar) overnight at 4°C. Secondary antibody incubation was performed for 2h at room temperature, then samples were washed several times in PBS 0.5% Triton X-100. Next, samples were gradually dehydrated in ethanol baths (50%, 80%, 95%, 100%) for at least 20min each at room temperature. Samples were incubated in 100% ethanol overnight at 4°C. Samples were further incubated in hexane (Sigma-Aldrich-Merck) for 2h before clearing in benzyl alcohol:benzyl benzoate (1:2) (Sigma-Aldrich-Merck). Samples were stored in this solution at room temperature and protected from light.

## Immunostaining

For retina and brain sections, samples were first defrosted and washed three times 10min with PBS. Samples were saturated in a blocking solution (3% bovine serum albumin (BSA) (Sigma-Aldrich), 5% donkey serum (Merck Millipore), 0.5% Triton X-100 (Sigma-Aldrich) in PBS) for 1h at room temperature and then incubated overnight at 4°C with primary antibodies: anti-melanopsin (Abcam, 1:500), anti-GFP (Abcam, 1:500), anti-RBPMS (Merck Millipore, 1:400), anti-VIP (Immunostar, 1:400), anti-VGLUT2 (Abcam, 1:500), anti-PSD95 (Abcam, 1:500), anti-c-fos (Cell Signaling Technology, 1:200), ), anti-CART (R&D Systems, 1:300), anti-Neurofilament H (BioLegend, 1:400), anti-parvalbumin (Abcam, 1:300), anti-FOXP2 (Abcam, 1:400), anti-osteopontin (R&D Systems, 1:500). The following day, three washes of 10min with PBS 0.1% Triton X-100 were carried out before incubation for 2h with secondary antibodies diluted 1:500 in blocking solution: Alexa 488 anti-chicken (Jackson), Alexa 488 anti-goat (ThermoFisher Scientific), Alexa 488 anti-rabbit (ThermoFisher Scientific), Alexa 568 anti-rabbit (ThermoFisher Scientific), Alexa 647 anti-rabbit (ThermoFisher Scientific), Alexa 647 anti-guinea pig (Jackson), Alexa 647 anti-mouse (ThermoFisher Scientific), Alexa 568 anti-mouse (ThermoFisher Scientific). Sections were washed three times for 10min and then mounted with Fluoromount-G with DAPI mounting medium (ThermoFisher Scientific).

Whole-mount retinas were washed three times 10min in PBS, then blocked in PBS 0.5% Triton X-100 5% donkey serum for 1h at room temperature. Primary antibodies used were anti-melanopsin (Abcam, 1:300), anti-tubulin β3 (Tuj1, Biolegend, 1:500), anti-osteopontin (R&D Systems, 1:200), anti-CART (R&D Systems, 1:400), anti- Neurofilament H (BioLegend, 1:400). After three 10min-washes in PBS 0.1% Triton X-100, secondary antibodies were incubated respectively overnight at 4°C and for 2h at room temperature. After three 10min-washes in PBS 0.1% Triton X-100, retinas were mounted with Fluoromount-G with DAPI (ThermoFisher Scientific).

For growth cone immunostaining, retina explant cultures were fixed by adding an equal volume of 3% sucrose 8% PFA in culture medium, with 15min incubation. After three washes in PBS, explants were incubated overnight in PBS 3% BSA with primary antibody: anti-Robo1 (R&D Systems, 1:400) or anti-Robo2 (gift from Dr Alain Chédotal, 1:500), and anti-Tuj1 (Biolegend, 1:800). After three washes with PBS, secondary antibodies with Alexa 647-conjugated phalloidin (ThermoFisher Scientific, 1:500) were incubated for 2h. After PBS washes, explants were mounted with Fluoromount G with DAPI (ThermoFisher Scientific).

For co-cultures, samples were fixed by adding an equal volume of 3% sucrose 8% PFA in culture medium, with 15min incubation. Explants were washed three times in PBS and then permeabilized 10min in PBS 0.1% Triton X-100. Primary antibodies (anti-Tuj1, Biolegend, 1:400) and secondary antibodies were diluted in blocking solution (0.1% Triton X-100, 3% BSA, 5% donkey serum in PBS) and samples were incubated respectively for 2h and for 1h at room temperature. After PBS washes, samples were mounted with Fluoromount-G with DAPI (ThermoFisher Scientific).

## In Situ Hybridization

In situ hybridization (ISH) on sections was performed as described.[66] For chromogenic in situ hybridization (ISH), slices were incubated with digoxigenin (DIG)-labeled probes for *Ephb1*, *Netrin1*, *Nrcam*, *Plexina1*, *Robo1*, *Robo2*, *Sema6d*, *Sfrp1*, *Sfpr2*, *Shh*, *Slit1*,

*Slit2*, *Slit3* or *Vegf* overnight at 65°C. After hybridization of the DIG-labeled probe on slides, the alkaline phosphatase-conjugated anti-digoxigenin antibody (Roche, 11093274910) was incubated overnight at room temperature. Alkaline phosphatase staining was probed with NBT-BCIP (Roche, 11681451001). For *Robo1* or *Robo2* fluorescent ISH, digoxigenin-labeling probes were amplified with horseradish peroxidase using Cy3.5 tyramide signal amplification kit (PerkinElmer) for 5 to 10 min. For *Slit2* fluorescent ISH, signal detection of alkaline phosphatase was performed using Fast Red and naphthol (Sigma-Aldrich, F4648).

### Quantitative PCR

For sample collection, 6-week-old mice wild-type mice received a bilateral ONC. After 28 days, both SCN were dissected from injured (28dpc) and uninjured (intact) mice. N=4-5 mice were used in each group. SCN were dissociated in Trizol (Ambion Life technologies) for total RNA extraction. 100ng of total RNA were used for reverse transcription using SuperScript II (Invitrogen). mRNA levels were assessed by qPCR (Biorad) for *Slit1*, *Slit2*, and *Slit3*, and normalized to *Gapdh* levels.

### Imaging

Immunofluorescence and fluorescence in situ hybridization (ISH) on sections were imaged with DragonFly spinning disk confocal microscope from Andor, with a 25x objective. Chromogenic ISH on sections were imaged using Zeiss Slide Scanner Axio Scan.Z1. Co-cultures were imaged with epifluorescence microscopy (Nikon Ti Eclipse, 4x objective). Robo immunofluorescence in growth cones and VGLUT2/PSD95 immunofluorescence in SCN were imaged using a confocal microscope (LSM710, Zeiss), with a 63x objective (oil immersion, numerical aperture = 1.4) and AiryScan mode. AiryScan imaging yielded a resolution of ~140nm in *xy* and ~400nm in *z*. Whole-cleared optic nerves, chiasm and SCN were imaged with DragonFly spinning disk confocal microscope from Andor, with a 20x objective. Images were acquired with 2μm-thick z-stack and were automatically stitched using Fusion software or with Imaris stitcher, then visualized and analyzed with Imaris software. $CTB^+$ signal was segmented manually using Syglass software in virtual reality. SCN were segmented using $DAPI^+$ signal on Imaris and fibers inside the SCN were segmented on Imaris. Movies were produced with Imaris and annotated with Adobe Premier Pro.

### Behavioral assay

For assessment of circadian rhythms, we monitored wheel-running activity of mice housed in a 12h light/dark cycle. Under normal conditions, mice exhibit modest sex-dependent differences in behavioral parameters of circadian activity.[70] In this study, we chose to consider only females because of their higher voluntary physical activity[71] and faster resynchronization to external light/dark cycles after phase shift.[72] Groups consisted in 4 $Pten^{fl/fl}$ $SOCS3^{fl/fl}$ mice, 4 $Pten^{fl/fl}$ $SOCS3^{fl/fl}$ $Robo1^{-/-}$ $Robo2^{fl/fl}$ mice and 4 wild-type mice. Each mouse was housed individually in a cage equipped with a connected wheel allowing to record spontaneous activity (Intellibio Innovation). Recordings were performed every week from the time of injection, and restricted to 72h to exclude surgeries, recovery time and litter changing. When not recorded, mice were still in presence of a running wheel. Data were acquired every 15min with ActiWheel software (Intellibio Innovation) and analyzed with ActogramJ.[73] For analysis, distance (in cm) was plotted versus time. The Chi-2 periodograms allowed to estimate the period for each recording session. Activity onset was assessed as the average time of starting activity across two or three 24h-recording periods. Recordings showing zero activity across a full period were excluded from analysis.

## QUANTIFICATION AND STATISTICAL ANALYSIS

### Quantification of guidance defects and SCN reinnervation

Whole-cleared optic nerves, chiasm and SCN were imaged using DragonFly spinning disk confocal microscope (Andor) with a 20x objective. Images were acquired with 2μm-thick z-stack and were automatically stitched using Fusion software (20% tile overlap). All quantifications were assessed using Imaris software (version 9.6, Bitplane). For the number of axons reaching the chiasm, we counted $CTB^+$ fibers intersecting the XZ orthogonal section at the distal end of the ipsilateral optic nerve (ION). For the number of axons entering the SCN, we counted $CTB^+$ fibers intersecting the XZ median orthogonal section of both SCN. For all others regions (Figure S1), we proceeded the same way, using the oblique- (YZ oblique section at the midline for the chiasm) or ortho- (XZ orthogonal section at the proximal part of the optic tracts) slicers tools. Guidance defects in Figure S1 are presented as a percentage of regenerating axons by dividing the number of intersects in regions of interest by the axon number found at the distal end of the ION.

### Quantification of RGC survival

Eyes from intact, 3 days post-crush (dpc), 14dpc and 28dpc $Pten^{fl/fl}$ $SOCS3^{fl/fl}$ mice (previously injected with AAV2-Cre/CNTF/c-myc) were collected and post-fixed in 4% PFA solution overnight at 4°C. Tissue were prepared and stained with anti-melanopsin and anti-RBPMS antibodies as described above. Using Zeiss Slide Scanner Axio Scan.Z1, retina slices were imaged with 20x objective. For each animal, $melanopsin^+$ cells were counted on 5 retina sagittal sections centered around the optic nerve head and summed up. Using anti-RBPMS staining, we assessed the retina length of all retina sections. The sum of $melanopsin^+$ cells number for each animal was normalized to the length of retina section (in cm). For each condition, the $melanopsin^+$ cell survival was calculated by dividing the average $melanopsin^+$ cell number of each animal by the average of intact condition. For other RGC subpopulation markers (Figure S5), we considered two representative fields per section, on 2-3 sections for each animal (N=4 independent retinas). For each marker, we counted positive cells and normalized this number to the length of the ganglion cell layer. We calculated the survival rate of each marker-positive RGC subpopulation by dividing the numbers by the average number in intact condition.

### Quantification of OPN4-GFP$^+$ fibers in the SCN

50μm longitudinal sections of the SCN were prepared from Pten$^{fl/fl}$ SOCS3$^{fl/fl}$ Robo1$^{-/-}$ Robo2$^{fl/fl}$ OPN4-GFP mice at 28dpc and imaged as a z-stack with a z-step of 1μm, using DragonFly spinning disk confocal microscope (Andor) with a 25x objective. For each animal (N=3), CTB$^+$/GFP$^+$ fibers were counted on 3 adjacent sections spanning the SCN and summed up to estimate the number of OPN4-GFP$^+$ fibers entering the SCN.

### Quantification of Slit2 knockdown in the SCN

After *Slit2* fluorescent ISH, brain sections were immunolabeled with anti-Cre antibody (Biolegend, 1:500). Brain sections were imaged with epifluorescence microscopy (Nikon Ti Eclipse, 10x objective). The SCN region was manually drawn from the DAPI signal. *Slit2* fluorescence intensity was determined as the mean gray value in this region of interest. For each section, the fluorescence intensity was also determined in the optic chiasm (as a region with no specific staining, see Figure S3) and this value was subtracted from the SCN value. For each individual SCN, the resulting fluorescence intensity was averaged on two sections. Results are presented as a percentage of the control condition.

### Quantification of CTB retrograde labeling in the retina

Two weeks after CTB injection in the chiasm, mice were sacrificed and retinas were dissected, fixed and immunolabeled for anti-tubulin β3 (Tuj1, Biolegend, 1:500) and anti-melanopsin (Abcam, 1:300). For each animal (total N=4 independent retinas), 10-12 randomly selected fields were imaged using DragonFly spinning disk confocal microscope (Andor) with a 25x objective. For each mouse, CTB$^+$ and CTB$^+$/melanopsin$^+$ RGC were quantified and averaged per field. The total number of CTB$^+$ and CTB$^+$/melanopsin$^+$ RGC was estimated in proportion of the total area of a whole-mount retina, with 1 field ∼0.2594mm$^2$ and 1 retina ∼14mm$^2$ (consistent with Claes and Moons[74]), so ∼54 times the average per field.

### Co-culture data analysis

For each co-culture, the retina and the SCN explants (or COS aggregates) were manually annotated using ImageJ and the proximal and distal regions were defined as the 90°-angle portion of retina explant towards and away from the SCN explant or COS aggregate, respectively. Axon outgrowth was quantified in each region with a Sholl analysis using the ImageJ plug-in Neurite-J.[75] Background noise filtering was performed automatically and manually corrected. The number of neurite intersects was determined by the Sholl analysis with a step of 25μm. The guidance index is calculated as the $\log_2$-transform of the total number of intersects in the proximal region versus the distal region. With this index, a positive value represents attraction towards the source (SCN explant or COS aggregate), while a negative value represents repulsion away from the source, and a zero-value represents no preference. For statistical analysis, data were subjected to a one-sample t-test with a theoretical value of 0, using GraphPad Prism version 9.1.2.

### Quantification of c-fos-positive cell number and c-fos intensity

Brain sections were imaged for c-fos, CTB and DAPI using confocal imaging. For each animal, 4-6 serial sections spanning the SCN were quantified using ImageJ. Both SCN were manually defined using DAPI staining. In the c-fos channel, a Gaussian blur filter was applied (sigma = 3), then a threshold was manually applied to detect all c-fos-positive cells in the SCN. A Watershed was applied to detect individual cells, then the number of c-fos-positive cells was quantified with Analyze particles (minimum size = 9μm$^2$, circularity = 0.3-1.0) and the mean c-fos intensity was measured for each c-fos-positive cell. For each section, the threshold was subtracted from the cell average intensity. For each animal, the number of c-fos-positive cells and the c-fos intensity was averaged over all sections considered.

### Spatial point pattern analysis

To correlate CTB and c-fos distributions in SCN sections, a spatial point pattern analysis was performed. The SCN was manually defined from the DAPI channel. Individual events were automatically detected from the immunofluorescence confocal images using Qupath.[76] Multitype (CTB$^+$ and c-fos$^+$ events) point patterns were analyzed using spatstat R package.[43] Density maps with standard error intensity estimate were plotted. The G-cross function, i.e. the cumulative distribution of nearest neighbor distance from CTB$^+$ events to c-fos$^+$ events was plotted, taking into account the inhomogeneous distribution of each marker with the function Gcross.inhom.

### Statistical analysis

All quantitative data are represented as mean +/- standard error of the mean (s.e.m.). All statistical analysis were performed using GraphPad Prism software version 8. Normal distribution of the data was assessed using a Shapiro-Wilk test. Student's t-test for two conditions or one-way ANOVA with Dunnett's correction for at least three conditions were performed. For behavioral assay, Chi-2 periods and activity onset shift were compared with two-way ANOVA with Sidak's correction. The difference between two averages were considered significant when the p-value was strictly below 0.05, with the following usage: * p-value < 0.05; ** p-value < 0.01; *** p-value < 0.001; and ns: p-value ≥ 0.05, not significant.